Dielectric Spectroscopy of Ferromagnetic Semiconductors*

P. A. MILES, W. B. WESTPHAL, AND A. VON HIPPEL

Laboratory for Insulation Research, Massachusetts Institute of Technology, Cambridge, Massachusetts

TABLE OF CONTENTS

* Sponsored by the Office of Naval Research, the Army Signal Corps, the Air Force, and the Army Ordnance under contracts Nonr-1841(10) and AF 33(616)-2191.

INTRODUCTION

MODERN technology depends to a large extent on ferromagnetic materials for distribution, control, and utilization of power, for high-speed computers, and electronic devices of all kinds. A new perspective for high-frequency circuitry was opened up by the development of the ferrites or ferrospinels, materials with the general formula $M^{++}Fe_2O_4$, at the Philips Research Laboratories.[1] Lately, ferromagnetic semiconductors of hexagonal,[2] as well as cubic, perovskite,[3] and garnet[4] structures have made their appearance. Like numerous other research groups, the Laboratory for Insulation Research has been active in the study of these materials over the last few years. In particular it concerns itself with their response to electric and magnetic excitations over a very broad frequency range, extending, with gaps, from dc to the ultraviolet. This review aims at a unified appraisal of the information obtained by such a broad-band approach. In the absence of an accepted name we call this effort "dielectric spectroscopy."

The stirring sequence of spectral lines, shown by individual atoms and molecules and described by the Rydberg-Ritz combination principle, led to an understanding of the quantum states of electronic excitation, vibration and rotation. These resonance spectra of individual particles extend from the x-ray into the microwave region. By condensing gases to liquids and solids, the frequency range of the electrical engineer from microwaves to dc fills up with absorption spectra, and drastic changes occur in the optical spectral range. The characteristic response of the individual particles to the electromagnetic field becomes submerged in effects of mutual interaction.

In consequence, the original sharpness of the resonance response of atoms and molecules with its revealing detail is supplanted in liquids and solids by broad resonance and relaxation spectra with much more scrambled information. Only the nuclear and paramagnetic resonance spectra may still transmit fine and hyperfine structure intelligence, because the magnetic spins are loosely coupled to their surroundings.

[1] J. L. Snoek, *New Developments in Ferromagnetic Materials* (Elsevier Publishing Company, New York and Amsterdam, 1947).
[2] Went, Rathenau, Gorter, and van Oosterhout, Philips Tech. Rev. **13**, 194 (1952).
[3] G. H. Jonker and J. H. van Santen, Physica **16**, 337 (1950).
[4] R. Pauthenet, Compt. rend. **242**, 1859 (1956).

The spectroscopist has always considered the optical range from infrared to ultraviolet as his domain and has added in recent years microwave and magnetic spectroscopy as far as they are concerned with resonance lines and therefore amenable to his old language. The electrical engineer, by necessity, has measured the dispersion and absorption of materials from dc to microwaves, but essentially from the empirical standpoint of knowing these characteristics for applications. Only the relaxation spectra caused by the orientation of permanent electrical dipole moments, first interpreted by Debye, have become an important and widely used source of molecular information, especially for chemical problems.

Obviously, for a true understanding of liquids and solids the total range from dc to x-rays should be considered as a unified stage on which the interplay between electromagnetic fields and matter is enacted.

1. THE LANGUAGE OF DIELECTRIC SPECTROSCOPY[5]

The name "dielectric," as used here, refers to any material when viewed from the standpoint of electric or magnetic response. In their reaction to sinusoidal electric and magnetic fields, dielectrics can be characterized by their *complex permittivity* and *complex permeability*,

$$\begin{aligned}\epsilon^* &= \epsilon' - j\epsilon'' \\ \mu^* &= \mu' - j\mu''.\end{aligned} \tag{1.1}$$

These parameters, the real permittivity (dielectric constant) ϵ' and permeability μ', describing the storage of electric and magnetic energy and the loss factors ϵ'' and μ'' its dissipation, are actually measured in reference to vacuum as a *relative* complex permittivity and permeability

$$\begin{aligned}\frac{\epsilon^*}{\epsilon_0} &\equiv \kappa^* = \kappa' - j\kappa'' \\ \frac{\mu^*}{\mu_0} &\equiv \kappa_m{}^* = \kappa_m{}' - j\kappa_m{}''.\end{aligned} \tag{1.2}$$

In the rationalized mks system, used here, the dielectric constant and permittivity of free space are

$$\begin{aligned}\epsilon_0 &= 10^7/4\pi c^2 \simeq 8.854\times10^{-12} \quad [\text{farad/m}] \\ \mu_0 &= 4\pi\times10^{-7} \simeq 1.257\times10^{-6} \quad [\text{henry/m}]\end{aligned} \tag{1.3}$$

in which, when precision values are needed, c is the experimental value of the velocity of light in vacuum expressed in meters per second. For most practical purposes one may set $c=3\times10^8$ m/sec which is sometimes called the standardized velocity of light. From the product and ratio of these we get the velocity of light c and the impedance of free space Z

$$\begin{aligned}c &\equiv (\epsilon_0\mu_0)^{-\frac{1}{2}} \simeq 3\times10^8 \quad [\text{m/sec}] \\ Z &\equiv (\mu_0/\epsilon_0)^{\frac{1}{2}} \simeq 120\pi = 376.6 \quad [\text{ohm}].\end{aligned} \tag{1.4}$$

Permittivity and permeability, as defined, refer to isotropic, linear dielectrics; that is, an electric field **E** creates a polarization **P** and a magnetic field **H** a magnetization **M** parallel and proportional to such field. The electric flux density **D** and the magnetic flux density **B** are the arithmetic sum of field lines and dipole chains,

$$\begin{aligned}\mathbf{D} &= \epsilon_0\mathbf{E} + \mathbf{P} = \epsilon^*\mathbf{E} \\ \mathbf{B} &= \mu_0\mathbf{H} + \mu_0\mathbf{M} = \mu^*\mathbf{H}.\end{aligned} \tag{1.5}$$

The complex nature of the permittivity and permeability indicates a temporal phase shift between the acting field, **E** or **H**, and the dipole moment per unit volume, **P** or **M**, created by such field. The product of angular frequency and electric-loss factor represents a *dielectric conductivity*

$$\sigma = \omega\epsilon''[\text{ohm}^{-1}\text{m}^{-1}], \tag{1.6}$$

which may correspond to a true conductivity created by migrating charge carriers or to any other dissipative action of the polarization.

Alternative sets of parameters, frequently used in science and engineering, can easily be expressed in terms ϵ^* and μ^*. The propagation of electromagnetic waves is described by a complex propagation factor

$$\gamma \equiv \alpha + j\beta = j\omega(\epsilon^*\mu^*)^{\frac{1}{2}}, \tag{1.7}$$

with α designating the attenuation factor and β the phase factor of the wave. The intrinsic impedance

$$Z_i \equiv \frac{E}{H} = \left(\frac{\mu^*}{\epsilon^*}\right)^{\frac{1}{2}} \tag{1.8}$$

of the dielectric represents the ratio of the coupled electric and magnetic field components as to amplitude and temporal phase for an infinitely extended material. Wavelength λ and phase velocity v in the dielectric are given as

$$\begin{aligned}\lambda &= \frac{2\pi}{\beta} \\ v &= \nu\lambda = \frac{\omega}{\beta}.\end{aligned} \tag{1.9}$$

The ratio of wavelength or phase velocity in vacuum to that in the dielectric material is the index of refraction

$$n \equiv \frac{\lambda_0}{\lambda} = \frac{c}{v} = \frac{\lambda_0}{2\pi}\beta, \tag{1.10}$$

[5] For a systematic development of the electric and magnetic concepts see A. von Hippel, *Dielectrics and Waves* (John Wiley and Sons, Inc., New York, 1954, and Technology Press, Massachusetts Institute of Technology).

and the attenuation per radian, the index of absorption,

$$k \equiv \frac{\alpha\lambda}{2\pi} = \frac{\alpha}{\beta}. \tag{1.11}$$

The indices of refraction and absorption together define the complex index of refraction

$$n^* \equiv n(1 - jk), \tag{1.12}$$

which the physicist uses for the characterization of materials in place of the propagation factor of the engineer,

$$\gamma = j\frac{2\pi}{\lambda_0} n^*. \tag{1.13}$$

The relations between flux densities and fields, measured by permittivity and permeability [see (1.5)], contain also the contribution of the field *in vacuo*. One refers to the dipole response of the material alone by introducing the electric and magnetic susceptibilities χ and χ_m:

$$\begin{aligned} \mathbf{P} &= (\epsilon' - \epsilon_0)\mathbf{E} \equiv \chi\epsilon_0\mathbf{E} \\ \chi &= \frac{\mathbf{P}}{\epsilon_0\mathbf{E}} = \kappa' - 1 \\ \mathbf{M} &= \left(\frac{\mu' - \mu_0}{\mu_0}\right)\mathbf{H} \equiv \chi_m\mathbf{H} \\ \chi_m &= \frac{\mathbf{M}}{\mathbf{H}} = \kappa_m' - 1. \end{aligned} \tag{1.14}$$

In anisotropic, linear dielectrics, **P** and **M** are not, in general, parallel to the generating fields; hence each component of **D** or **B** is a linear function of the three space components of **E** or **H** as

$$\begin{aligned} D_1 &= \epsilon_{11}E_1 + \epsilon_{12}E_2 + \epsilon_{13}E_3, \\ D_2 &= \epsilon_{21}E_1 + \epsilon_{22}E_2 + \epsilon_{23}E_3, \\ D_3 &= \epsilon_{31}E_1 + \epsilon_{32}E_2 + \epsilon_{33}E_3, \end{aligned} \tag{1.15}$$

and

$$\begin{aligned} B_1 &= \mu_{11}H_1 + \mu_{12}H_2 + \mu_{13}H_3, \\ B_2 &= \mu_{21}H_1 + \mu_{22}H_2 + \mu_{23}H_3, \\ B_3 &= \mu_{31}H_1 + \mu_{32}H_2 + \mu_{33}H_3. \end{aligned} \tag{1.16}$$

Because of the purely displacive nature of the polarization process the permittivity tensor is symmetric with $\epsilon_{ij} = \epsilon_{ji}$. The same is true of the permeability tensor at frequencies well below the inverse of the relaxation time associated with the return to equilibrium of a disturbed magnetic system. At higher frequencies, however, $\mu_{ij} = -\mu_{ji}$ for $i \neq j$. The skew symmetry of these elements reflects the gyroscopic nature of the magnetization process (Sec. 6). A possible maximum of six independent coefficients of permittivity and of permeability therefore exists. How many are not zero and different from each other, depends on the macroscopic symmetry of the system. Frequently more useful for the molecular analysis are the corresponding susceptibility matrices

$$\chi = \left\| \begin{matrix} \chi_{11} & \chi_{12} & \chi_{13} \\ \chi_{21} & \chi_{22} & \chi_{23} \\ \chi_{31} & \chi_{32} & \chi_{33} \end{matrix} \right\|. \tag{1.17}$$

Notwithstanding the tensor form of ϵ^* and μ^* in anisotropic crystals, the behavior of a polycrystalline aggregate of such materials is described by the simple quantities $\epsilon^* = \epsilon' - j\epsilon''$, $\mu^* = \mu' - j\mu''$, provided that the microstructure of the material is much smaller than the specimen size and the wavelength of the exciting field, and provided that the material is in a depolarized or demagnetized state.

For ferroelectrics and ferromagnetics the situation becomes more involved because the moments line up spontaneously, forming electric or magnetic axes. Changes in position cause, in general, a crystal deformation, hence a coupling exists to the elastic coefficients of the crystal structure (piezoelectricity and piezomagnetism†). Furthermore, the response to external fields is nonlinear and depends on the prehistory of the sample because domain arrays are formed to minimize the field energy.

Ferroelectrics and ferromagnetics are thus characterized by polarization and magnetization curves depending on field strength, and the permittivity and permeability coefficients here used designate certain slopes of these characteristics (Fig. 1.1). In evaluating

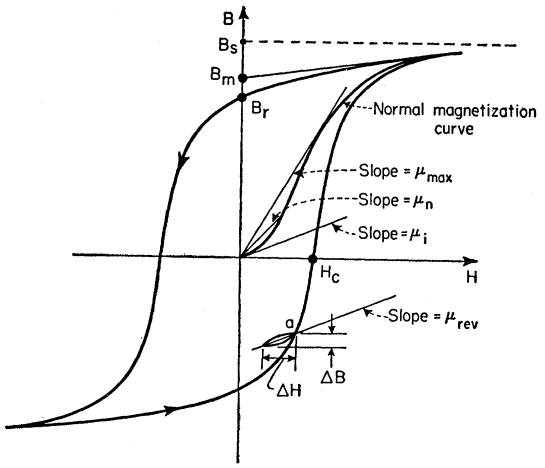

FIG. 1.1. Parameters characterizing the quasi-static magnetization of ferromagnetics.

† The term "piezomagnetism" is becoming rightfully accepted in place of "magnetostriction," because in ferromagnetics the effect is analogous to the piezoelectricity of ferroelectrics. The terms "electrostriction" and "magnetostriction" should be reserved to the mechanical deformation caused by induced moments. These latter processes have no inverse, i.e., mechanical deformation does not in this case produce or alter moments as a first-order effect.

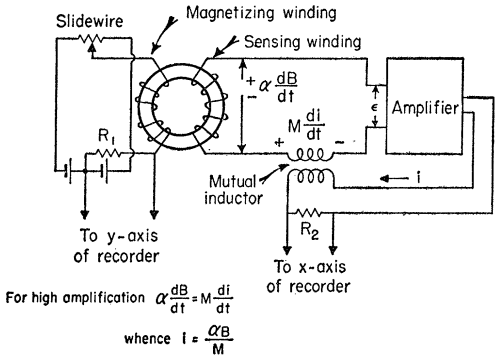

FIG. 2.1. Recording fluxmeter for quasi-static magnetic measurements.

"normal" curves and hysteresis loops, corrections are required to transform from the externally applied field strength $\mathbf{E}$ or $\mathbf{H}$ to the internally applied field strength $\mathbf{E}_i$ and $\mathbf{H}_i$. The shape of the sample enters because the free poles at the sample boundaries produce depolarizing and demagnetizing fields. For ellipsoids of revolution the internal field is homogeneous and derived from the applied field as

$$\begin{aligned} \epsilon_0\mathbf{E}_i &= \epsilon_0\mathbf{E}-w\mathbf{P} \\ \mathbf{H}_i &= \mathbf{H}-w\mathbf{M}, \end{aligned} \tag{1.18}$$

where w is a shape factor varying from zero for a long needle parallel to the field, to one for a disk perpendicular to the field.

As mentioned at the beginning of this section, we use the rationalized mks system. The conversion factors of the magnetic field strength and flux density to the oersted and gauss are

$$\begin{aligned} [\mathbf{H}]=[\text{amp/m}] &= \frac{4\pi}{10^3}[\text{oersted}] \\ &\simeq 1.26\times 10^{-2}[\text{oersted}] \\ [\mathbf{B}]=[\text{weber/m}^2] &= 10^4[\text{gauss}]. \end{aligned} \tag{1.19}$$

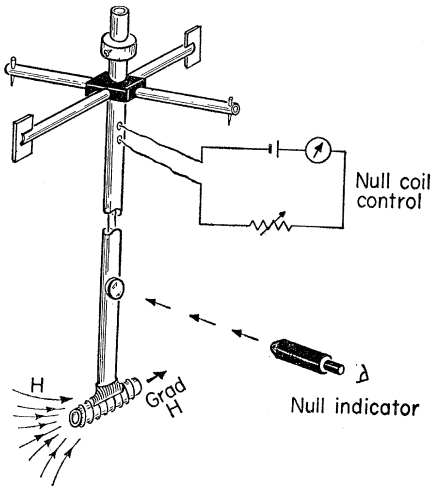

FIG. 2.2. Pendulum magnetometer.

2. MEASUREMENT TECHNIQUES

(a) Quasi-Static Magnetic Measurements

Up to ± 2000 amp/m (25 oersteds), our normal magnetization curves and hysteresis loops are plotted by a quasi-static fluxmeter (Fig. 2.1), developed after a design by Cioffi.[6] For fields up to 400 000 amp/m, the normal magnetization characteristics can be determined with a null-coil pendulum magnetometer[7] (Fig. 2.2). Finally, a vibrating-coil magnetometer has been developed here recently[8] (Fig. 2.3) for rapid measurements of magnetization and anisotropy characteristics, useful over a wide temperature and pressure range. With this instrument the dipole field of the sample can be measured at a distance, hence outside of and unhindered by thermostats or pressure bombs.

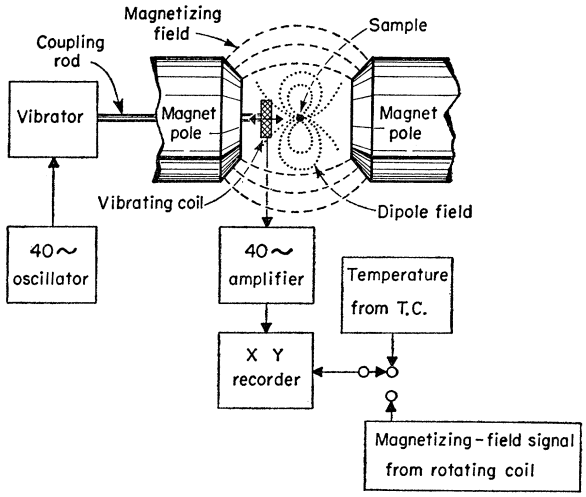

FIG. 2.3. Vibrating-coil magnetometer.

(b) Measurements of ε^* by Four-Terminal Methods

To avoid boundary-layer effects, semiconductors should be measured, in general, by a four-terminal arrangement. For dc the voltage drop across the potential electrodes is compared with that across a 10 000-ohm standard resistor (Fig. 2.4). Ac measurements up to 10^4 cps are made either with a differential voltmeter circuit (Fig. 2.5) or (to avoid the nonlinearity of the electronic components) in a potentiometer circuit with the coupling transformer to the detector tuned to resonance to provide a very high input impedance (Fig. 2.6).

(c) Two-Terminal Measurements of ε^* and μ^* at Low Frequencies (10^2 to 10^5 cps)

In most cases the permittivity is obtained by balancing the sample capacitor in one of the bridge circuits

[6] P. P. Cioffi, Rev. Sci. Instr. **21**, 624 (1950).
[7] C. A. Domenicali, Rev. Sci. Instr. **21**, 327 (1950).
[8] D. O. Smith, Rev. Sci. Instr. **27**, 261 (1956).

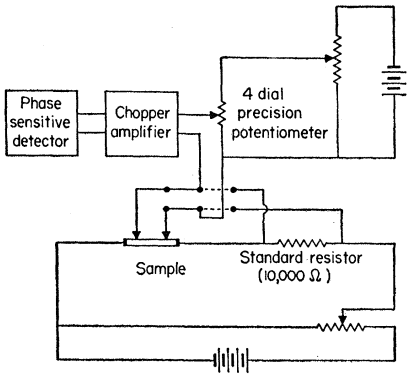

FIG. 2.4. Equipment for four-terminal dc conductivity measurements.

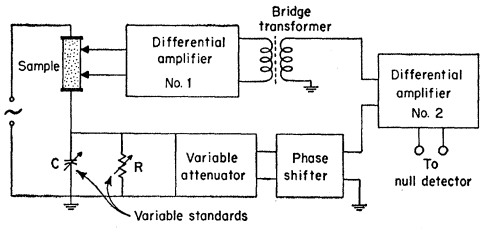

FIG. 2.5. Differential voltmeter circuit for four-terminal ac measurements up to 10^4 cps.

shown in Fig. 2.7. For permeability determinations toroid samples with windings are used and measured with a capacitance in series in the same type of bridge circuit (Fig. 2.8).

(d) ε^* and μ^* in the Medium-Frequency Range (10^5 to 10^8 cps)

Measurements of the permittivity on lumped-capacitor samples have been extended by the use of a susceptance variation circuit; dielectric constant and loss are obtained by the resonance position and half-width of the resonance curve (Fig. 2.9). For toroids in permeability determinations this technique is inferior because of the distributed capacitance of the windings. Hence the complex permeability is obtained on coaxial samples. For the range from 10^5 to 10^7 cps, such a sample is placed on a movable shorting plunger in a four-arm coaxial bridge (Fig. 2.10). Between 10^7 and 10^8 cps the coaxial sample can be measured at the

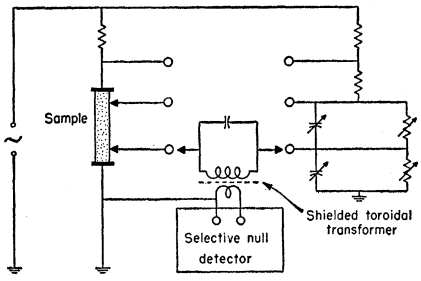

FIG. 2.6. Potentiometer circuit for four-terminal ac measurements.

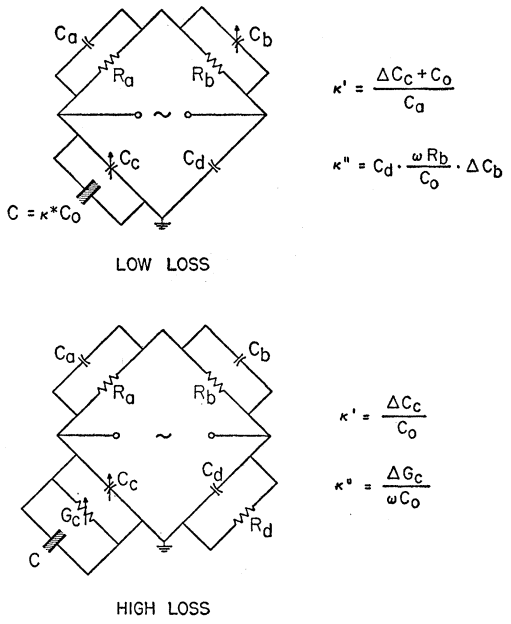

FIG. 2.7. Bridge circuits for electrical measurements from 10^2 to 10^5 cps.

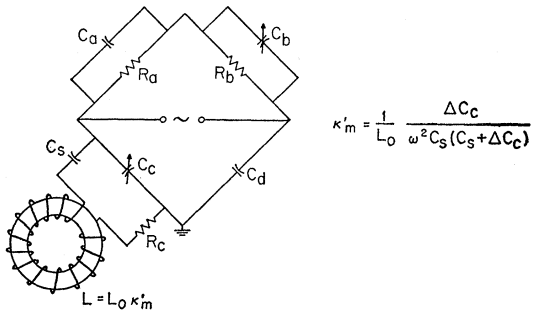

FIG. 2.8. Bridge circuit for magnetic measurements from 10^2 to 10^5 cps.

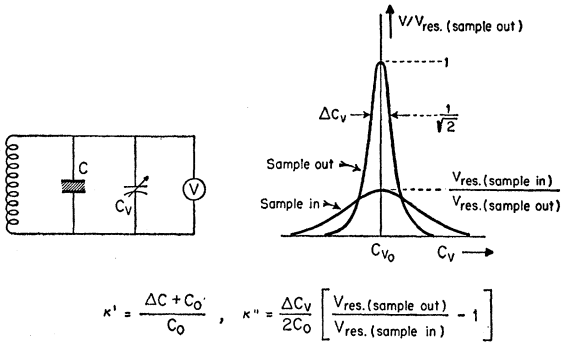

FIG. 2.9. Resonance circuit for electric measurements from 10^5 to 10^8 cps.

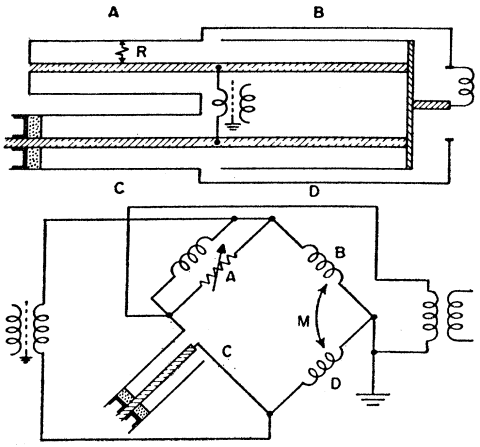

$$K'_m = \frac{\Delta\ell + d}{d} - \frac{\frac{\Delta\ell_R}{d}\left(\frac{Z_C}{R}\cdot\frac{2\pi\Delta\ell_R}{\lambda}\right)^2}{1+\left(\frac{Z_C}{R}\cdot\frac{2\pi\Delta\ell_R}{\lambda}\right)^2}$$

$$K''_m = \frac{\lambda}{2\pi d}\cdot\frac{\frac{Z_C}{R}\left(\frac{2\pi\Delta\ell_R}{\lambda}\right)^2}{\left(1+\frac{Z_C}{R}\cdot\frac{2\pi\Delta\ell_R}{\lambda}\right)^2}$$ Line loss neglected

FIG. 2.10. Coaxial line bridge for magnetic measurements from 10^5 to 10^7 cps.

shorted end of a fixed line section in the sample arm of a commercial radio-frequency bridge (G.R. 916-A or 1601) (Fig. 2.11).

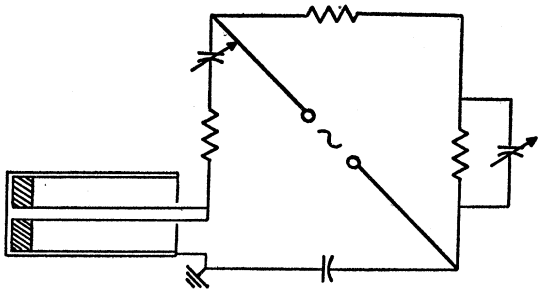

FIG. 2.11. Impedance bridge with coaxial line for magnetic measurements from 10^7 to 10^8 cps.

(e) Measurements in the High-Frequency Range (10^8 to 10^{10} cps)

Between 10^8 and 3×10^9 cps ϵ^* and μ^* are obtained in a coaxial line with standing-wave detector, by locating a thin sample in two successive measurements in a region of high magnetic and high electric field strength (short-circuit and open-circuit method) (Fig. 2.12). A dc magnetic field parallel to the high-frequency field can be superposed by connecting a current source across the center conductor. At higher frequencies, the standing-wave method is used with hollow wave guides.

(f) Measurements in the Optical Range

Absorption by the ferrites in the optical range is very high. Our spectra are recorded from 2000 to about 10 000 A by a Cary instrument and from 1 to about 40 μ by an IR-3 Beckman spectrophotometer, equipped for the far infrared with KRS-5 optics. For a survey study, ceramic or crystal samples were pulverized to particles of the order of 0.1 to 1 μ, mixed with KBr powder and pressed to nearly transparent specimens[9] in the form of disks (*ca* 1 cm diam, 2 mm thick). In addition, single-crystal disks were measured in reflection and evaporated layers in transmission.

3. STRUCTURE OF FERRITES

The ferrites considered here have the spinel structure, a closest-packed cubic array of O^{2-} spheres with compensating cations in interstitial positions. Adjacent to each oxygen ion are 14 interstices: 6 located in the cube-edge directions, surrounded by six oxygen ions (octahedral sites), 8 placed in the space-diagonal directions, surrounded by four oxygen ions (tetrahedral sites) (Fig. 3.1).

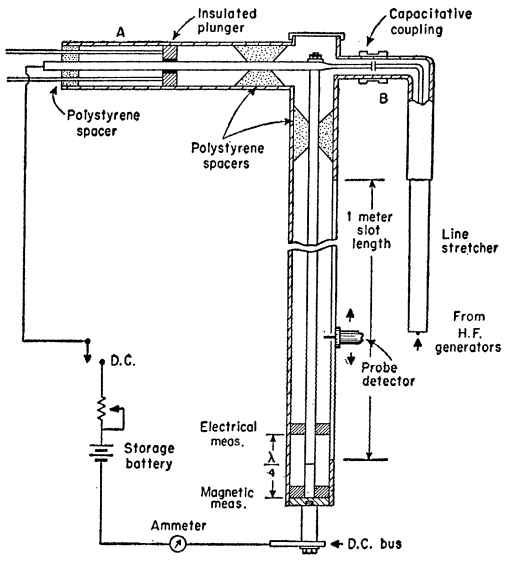

FIG. 2.12. Standing-wave method for electric and magnetic measurements from 10^8 to 10^{10} cps in presence of dc magnetic bias.

[9] M. M. Stimson and M. J. O'Donnell, J. Am. Chem. Soc. **74**, 1805 (1952); U. Schiedt and H. Reinwein, Z. Naturforsch. **7B**, 270 (1952).

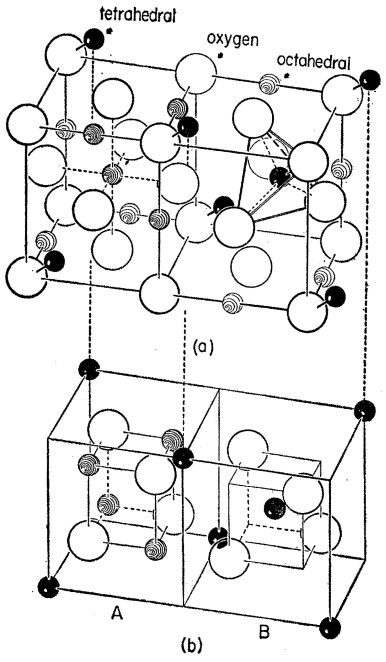

FIG. 3.1. Two views of spinel structure: (a) octahedral and tetrahedral sites; (b) repeating sections of unit cell.

The prototype of these ferromagnetic spinels is magnetite (Fe_3O_4). Here each anion is balanced by $\frac{3}{4}$ of a cation; hence, placing around each oxygen "a" cations in the octahedral and "b" cations in the tetrahedral positions, we have to fulfill the condition

$$\frac{a}{6}+\frac{b}{4}=\frac{3}{4}; \tag{3.1}$$

that is, $a=3$, $b=1$ or $a=0$, $b=3$. The cations repel each other and therefore should be placed at maximum possible separation. If, in addition, we require that a repetition of the oxygen-cation configuration in space should produce a symmetrical and stable lattice structure, the observed unit cell of magnetite results with 32 oxygens and 24 cations in the arrangement $a=3$, $b=1$. The unit cell comprises 8 Fe_3O_4 groups (Fig. 3.2).

Thus far we have assumed that three iron ions of equal valence ($Fe^{(8/3)+}$) compensate the negative charge of four oxygen ions. Actually, a chemist would write for magnetite $Fe_3O_4=Fe^{2+}O^{2-}Fe_2^{3+}O_3^{2-}$, that is, postulate 8 ferrous and 16 ferric ions per unit cell. In structures of the spinel type, the distribution of cations over the permissible sites may lie anywhere between the two extreme cases of 8 divalent ions on tetrahedral sites and 16 trivalent ions on octahedral sites (normal spinel) or 8 trivalent ions on tetrahedral sites and the remaining 8 divalent and 8 trivalent ions on octahedral sites (inverse spinel). The physicist finds[10] that, in magnetite, 8 Fe^{3+} ions are located in tetrahedral (A) sites (inverse spinel), but the sixteen remaining cations in the octahedral (B) sites can be separated only artifically at room temperature into 8 Fe^{3+} and 8 Fe^{2+} ions. The high conductivity of magnetite suggests that the electron exchange between the ferrous and ferric ions at identical lattice sites is so rapid ($\sigma\simeq 10^2$ ohm^{-1} cm^{-1}), that an average charge of $+2.5$ should be assigned to these iron atoms in octahedral positions.

Each iron ion is the carrier of a magnetic moment; hence the two different cation sites form two magnetic sublattices A and B. Néel[11] successfully explained the spontaneous magnetizations observed in simple ferrites by assuming that the predominant coupling between the magnetic moments of the cations is that between the

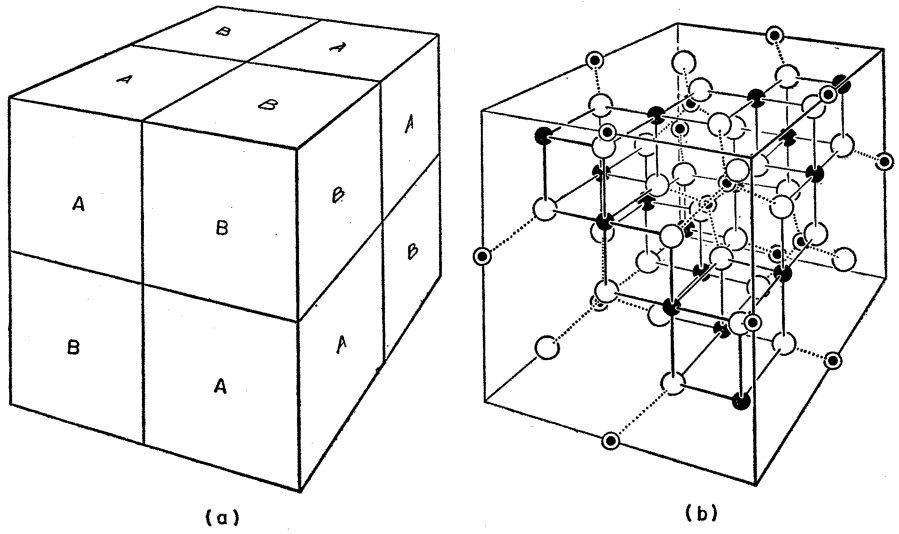

Fig. 3.2. Spinel unit cell: (a) stacking pattern of repeat units; (b) lattice.

[10] E. J. W. Verwey, Nature **144**, 327 (1939); E. J. W. Verwey and P. W. Haayman, Physica **8**, 979 (1941).
[11] L. Néel, Ann. phys. [12] **3**, 137 (1948).

tetrahedral and octahedral sublattices and that this $A \leftrightarrow B$ coupling is antiferromagnetic. Thus the saturation magnetization of magnetite at absolute zero should correspond to that of the ferrous ions only:

	B sites	*A* sites	
Filled cation sites per unit cell:	Octahedral (16)	Tetrahedral (8)	Resultant moment
Magnetic moments:	$8\,Fe^{++}\uparrow 8\,Fe^{+++}\uparrow$	$8\,Fe^{+++}\downarrow$	$8\,Fe^{++}\uparrow$.

The form of the magnetization *vs* temperature curve, on the other hand, depends essentially on the magnitude and nature of the couplings within each sublattice. In general these are found to be antiferromagnetic, although magnetite appears to have a weak ferromagnetic coupling between the ions of sublattice A.

Near 119°K, one observes an electronic order-disorder transition in magnetite. The electron exchange between Fe^{2+} and Fe^{3+} has obviously slowed down so much that the lattice can respond to the whereabouts of the electrons by distortion. Thus an ordered $Fe^{2+}Fe^{3+}$ structure can be frozen in at the B sites. In Néel's sense, we should now distinguish between one A and two B magnetic sublattices.

By substituting other cations for Fe^{2+} and/or Fe^{3+}, a great variety of materials of ferrite-type can be made in which the resulting magnetic properties depend in a complicated manner on the spin interactions in and between such sublattices. A satisfactory physical analysis of the ferrites requires accurate knowledge of the cation distribution, of the electron exchange between multivalent ions, of the origin and coupling of the magnetic moments, and an understanding of their interaction with the crystal lattice. In this connection it must be considered that a purely ionic description of the structure may not be justified.

4. PRINCIPLES OF DIELECTRIC ANALYSIS

At first sight, the broad-band spectrum of a ferrite evokes a feeling of complexity and inarticulation (Fig. 4.1). A number of effects are superposed and guiding principles are needed to reduce the integrated characteristics into meaningful components.

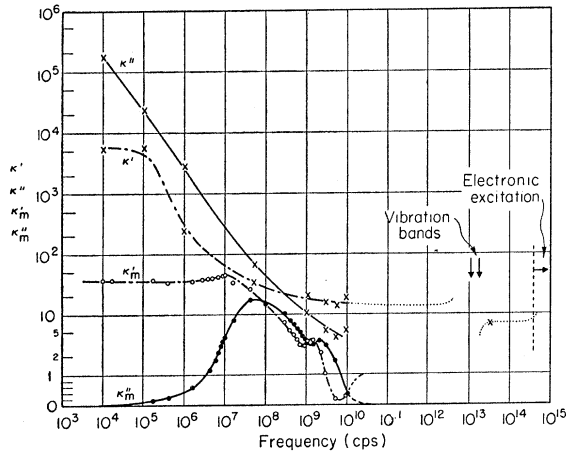

FIG. 4.1. Broad-band dielectric spectra of nickel ferrite (dispersion and absorption).

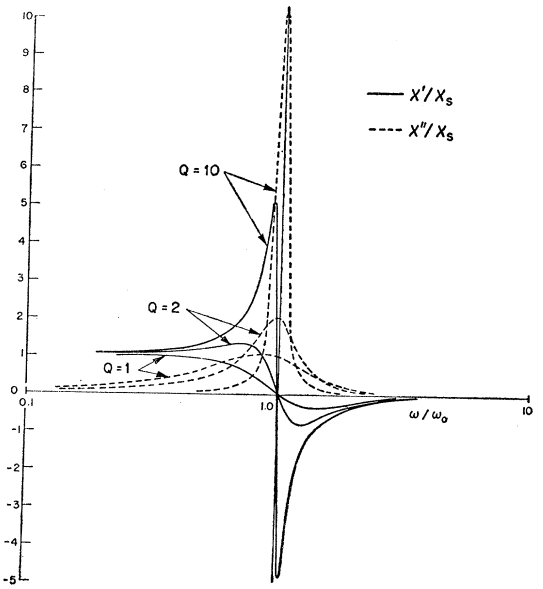

FIG. 4.2. Normalized susceptibility (dispersion and absorption) of classical resonator.

The response to electromagnetic fields is under consideration. Hence it is logical that we inquire about electric processes excited by electric fields, magnetic processes excited by magnetic fields, and interaction phenomena between the two. Furthermore, electromagnetic fields couple to matter essentially by dipole terms; hence charge carriers, induced moments, and permanent moments will make their appearance and respond in resonance and relaxation spectra. These spectra are characterized by the frequency response of their dispersion (κ') and absorption (κ'') components, but the identification as to type may be ambiguous, since a continuous transition from resonance to relaxation is possible.

The common classical resonator, a mechanical one with viscous damping or, electrically, a simple series LRC circuit, is identical in its frequency response with the quantum-mechanical resonator with its transitions between quantum states of isolated atoms and molecules.[12] If N is the number of resonators per unit volume, e their charge and m their mass, one observes an electric susceptibility [see (1.14)]

$$\chi^*=\kappa^*-1=\frac{Ne^2/\epsilon_0 m}{\omega_0^2-\omega^2+j\omega 2\alpha}, \tag{4.1}$$

or, with respect to the static susceptibility χ_s, a nor-

[12] See reference 5, pp. 161 ff.

malized susceptibility (Fig. 4.2)

$$\frac{\chi^*}{\chi_s}=\frac{1}{1-\left(\frac{\omega}{\omega_0}\right)^2+j\frac{\omega}{\omega_0^2\tau_l}}. \tag{4.2}$$

For low damping, the spectral line is symmetrical about the resonance frequency ω_0 with a width $\Delta\omega_h$ at half-power points given by the attenuation factor 2α

$$\Delta\omega_h=2\alpha=\frac{1}{\tau_l}. \tag{4.3}$$

τ_l is the *lifetime* of the excited state. In classical terms, the quality factor **Q** of the resonator, defined as the ratio of energy stored to that dissipated per half-cycle, is equal to $\omega_0/\Delta\omega_h$. Transitions between quantized magnetic states in isolated systems, described by the magnetic susceptibility, follow the same form.

Elimination of the acceleration term in the resonance equation leads to the simplest prototype of a relaxation spectrum (Fig. 4.3)

$$\frac{\chi}{\chi_s}=\frac{1}{1+j\omega\tau}, \tag{4.4}$$

where the *relaxation time* τ corresponds, for example, to Debye's ordering time of permanent dipoles in a viscous medium.[13] We can transform from (4.2) to

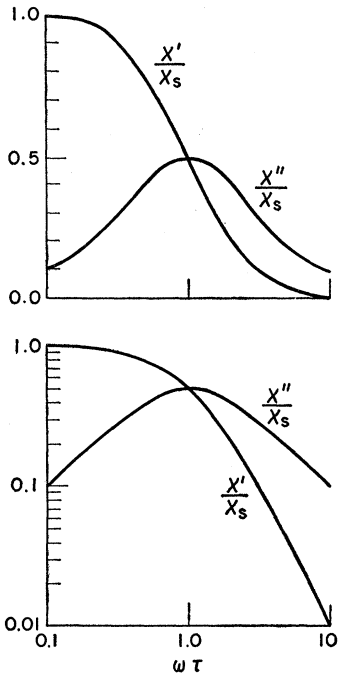

FIG. 4.3. Dielectric relaxation spectrum (dispersion and absorption).

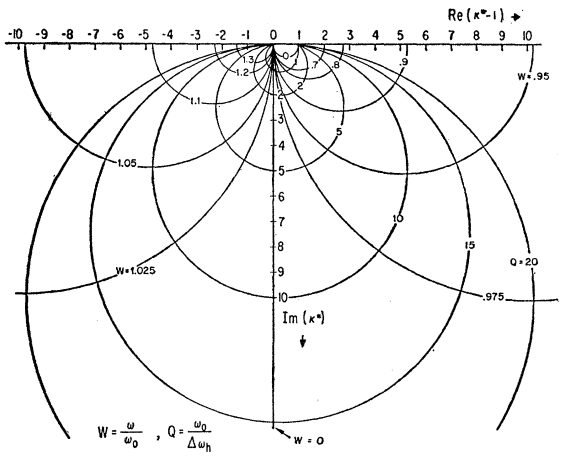

FIG. 4.4. Vector plot of the complex susceptibility (κ^*-1), illustrating continuous transition from resonance to relaxation spectrum.

(4.4) by defining formally

$$\tau=\frac{1}{\tau_l\omega_0^2}, \tag{4.5}$$

shifting the resonance to very high frequencies in comparison to the frequency of observation ($\omega\ll\omega_0$), and increasing the damping α, that is, reducing the lifetime τ_l until $\tau_l\ll(1/\omega_0)$. The physical meaning of this procedure is that we wipe out the discrete quantum states of the individual particles by interaction with their surroundings, and observe the adjustment of the particles in these surroundings. A typical example is the pressure broadening of spectral lines when a disrupting collision interferes before a vibration or rotation cycle can be completed. A plot of the vector χ^* (Fig. 4.4) shows the transition from a resonator (with the phase of its dipole moment relative to that of the inducing field varying from 0° to 180°) to the simple relaxing system with its circular arc locus (Cole-Cole plot[14]) and phase shift from 0° to 90°. The circular loci of Fig. 4.4 have the form

$$\left[\chi'-\frac{1}{2(1-w^2)}\right]^2+\chi''^2=\frac{1}{4(1-w^2)^2},$$

$$w=\frac{\omega}{\omega_0}=\text{constant}; \tag{4.6}$$

and

$$\left[\chi'-\frac{1-\sqrt{w}}{1-w^2}\right]^2+\left(\chi''-\frac{\mathbf{Q}}{2}\right)^2\simeq\frac{\mathbf{Q}^2}{4}\quad\text{for}\quad\mathbf{Q}>2.$$

Electron transitions and vibrations of individual particles find their counterpart in the electron transi-

[13] P. Debye, *Polar Molecules* (Chemical Catalog Company, New York, 1929), pp. 83 ff.

[14] K. S. Cole and R. H. Cole, J. Chem. Phys. **9**, 341 (1941).

tions and vibrations of coupled systems and hence maintain their resonance character. The rotation of electric dipoles in condensed systems leads to relaxation spectra, while the much looser coupling of electron and nuclear spins to their surroundings permits well-defined magnetic resonance spectra to persist. The experimental distinction between resonance and relaxation (Fig. 4.4) may be difficult, but two criteria, if fulfilled, unequivocally identify resonance. The dispersion curve of a relaxation spectrum can only fall with increasing frequency, hence a maximum or minimum of the κ' curve attests to a resonance contribution. Furthermore, the κ'' curve of the simple relaxation spectrum is the steepest absorption possible for this type. Plotted on a log-log scale it shows a maximum slope ± 1 (Fig. 4.3). Hence, a loss peak with a slope steeper than 1 is an unmistakable sign of resonance.

5. ELECTRIC SPECTRA

(a) Electronic Transitions

The absorption spectra of bound electrons in solids consist normally of a broad sequence of bands in the "eigenabsorption" region, correlated to specific transitions. They are preceded towards longer wavelengths by weaker absorptions arising from impurities and distorted lattice areas. Light absorption, especially at the tail of the intrinsic band, may lead to photoelectric conduction and to the buildup of new absorptions

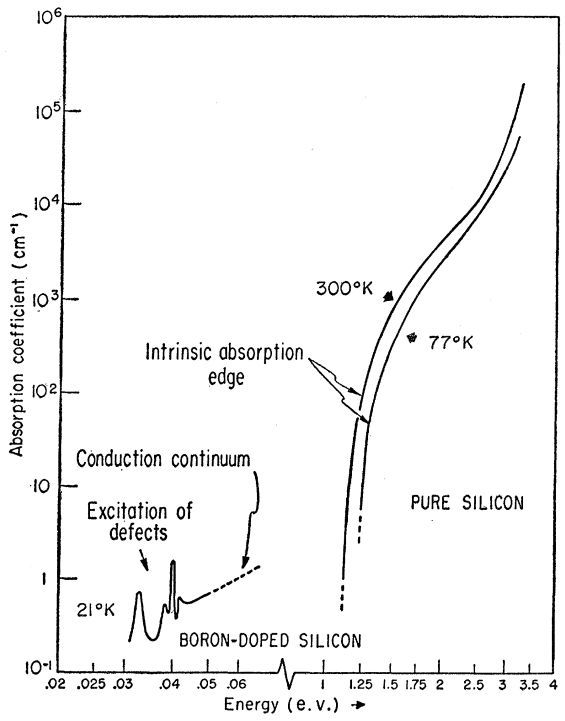

FIG. 5.1. Electronic absorption spectrum of silicon [W. C. Dash and R. Newman, Phys. Rev. **99**, 1151 (1955); R. Newman, *ibid.* **103**, 103 (1956)].

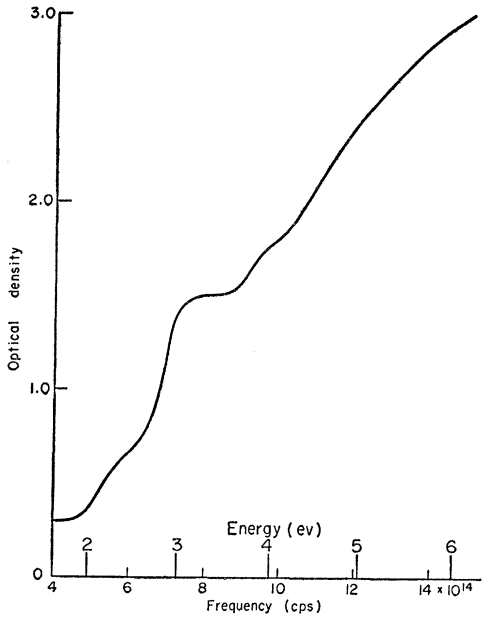

FIG. 5.2. Transmission of magnetite film in the optical region.

towards the infrared. Electronic conduction, to which the quantum-mechanical conduction band concept applies, will produce a continuum which underlies the other absorptions. Figure 5.1 illustrates these types of spectra for the case of impure silicon.

The ferrites considered here absorb strongly in the optical region. For this reason the information we possess at this time is limited. Transmission measurements on single crystals have to await development of grinding and etching techniques capable of reducing crystal sections to a thickness of about 0.1 micron. For a discussion of the low-frequency dielectric constant, it is necessary to know the over-all contribution of the electronic polarization. Estimates of this value are obtained from the refractive index of Mg ferrite at 0.6 micron ($\kappa' \simeq 6.5$) and by reflectivity measurements on a single crystal of nickel ferrite on the high-frequency side of the infrared bands ($\kappa' \simeq 7$). Thus the electronic polarization contributes a value of 6 to 7 to the static dielectric constant.

An actual transmission characteristic was taken on a magnetite film produced by the evaporation of pure iron and its oxidation to Fe_3O_4 (Fig. 5.2). Its scrambled information on transitions, for example, from cation *3d* levels to higher bands, or from O^{2-} to the various cations, points up the need for measurements on single crystals at very low temperatures in order to achieve resolution sufficient for the identification of individual lines.

(b) Infrared Vibrations

The unit cell of magnetite, as mentioned in Sec. 3 (Fig. 3.2), contains eight Fe_3O_4 groups or 56 particles,

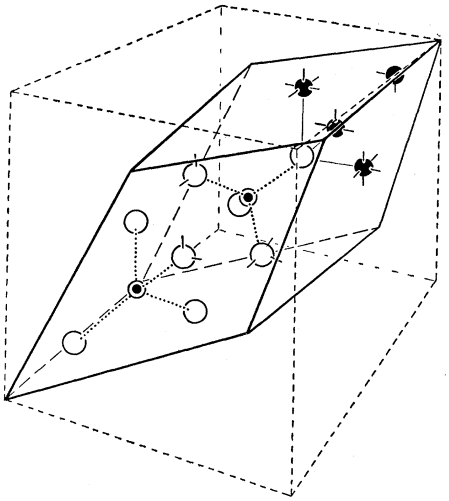

FIG. 5.3. Rhombohedral subcells of spinel lattice.

each of which contributes three degrees of freedom. Hence the unit cell has 168 normal vibrations. This inconveniently large number can be cut down by a factor of four by dividing the unit cell into four primitive rhombohedral subcells (Fig. 5.3). If we write the formula of the ferrites as MFe_2O_4, where M stands for a divalent metal ion, the rhombohedral cell ($M_2Fe_4O_8$) contains 14 ions which can be lumped into two MO_4 and one Fe_4 tetrahedral subgroups.

Of the 42 possible modes those which create a change in dipole moment $[(\partial \mathbf{u}/\partial r) \neq 0]$ are optically active. Only eight vibratory modes cause local dipole moment changes; three of these become inactivated because the over-all dipole-moment change in the primitive cell is zero; a fourth is a zero-frequency translation. Hence, four optically active modes remain and are in phase throughout the lattice, when the subcells are joined together.[15]

The mode of highest frequency (ν_1) corresponds to the vibrations of the oxygen ions along the tetrahedral bond directions, the [111] crystal directions; the next lower mode (ν_2) represents a motion of the oxygen ions in a direction almost perpendicular to the first one; the remaining two modes (ν_3, ν_4) correspond to oscillations of the metal ions in the force fields of their octahedral and tetrahedral oxygen environments (Fig. 5.4).

In absorption measurements, the real part α of the propagation constant γ is obtained. For a nonmagnetic material, γ may be expressed in terms of the dielectric constant $\kappa^*=\kappa'-j\kappa''$ as [Eq. (1.7)]

$$\gamma=\alpha+j\beta=\gamma_0\left(\frac{|\kappa^*|-\kappa'}{2}\right)^{\frac{1}{2}}+j\gamma_0\left(\frac{|\kappa^*|+\kappa'}{2}\right)^{\frac{1}{2}}. \quad (5.1)$$

However, when the material is powdered and imbedded in a loss-free dielectric, the absorption coefficient of the resultant mixture is measured. This is not simply the coefficient for the material, reduced in magnitude by the dilution, but depends on other factors. For example, pronounced scattering will occur when the particle sizes become of the order of the wavelength; the dielectric constant of the embedding medium also enters.[16] In the present work scattering becomes of importance only in the visible range. For particles very much smaller than the wavelength, the absorption is expected to follow the variations in the dielectric loss factor κ'' for the ferrite and to show peaks near the vibrational resonance frequencies.

Absorption spectra for six simple ferrites are shown in Fig. 5.4. Two main bands occur, with peaks in the vicinity of 550 and 400 cm^{-1}, which we attribute to the two highest modes; the two lower bands apparently lie beyond the range of our instrument. $ZnFe_2O_4$ is a "normal" spinel, that is, the Zn^{2+} ion occupies the tetrahedral lattice sites, while Fe_3O_4, $NiFe_2O_4$, and

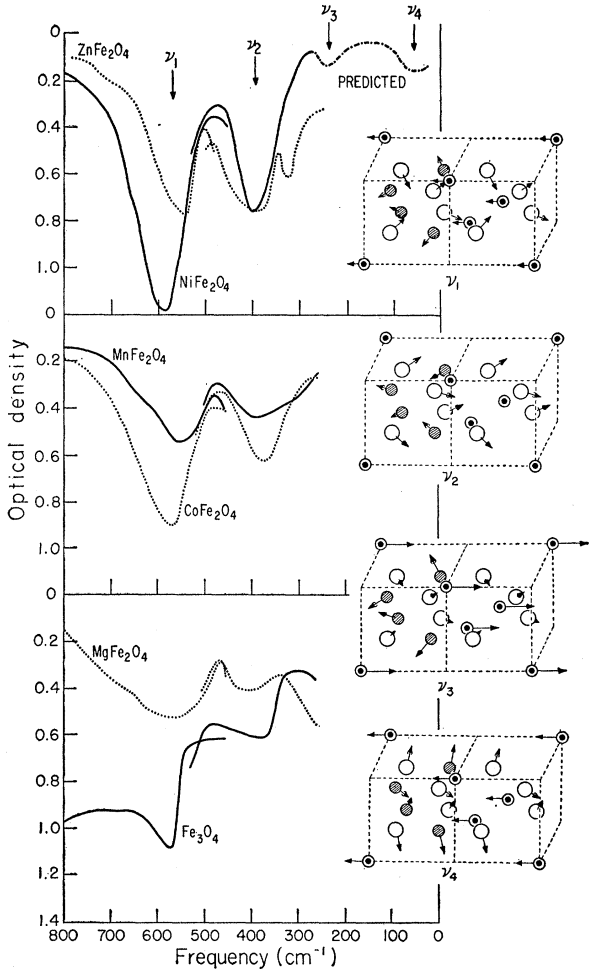

FIG. 5.4. Vibration spectra and associated active modes of ferrites (Waldron[15]).

[15] R. D. Waldron, Phys. Rev. **99**, 1727 (1955).

[16] J. T. Last, Phys. Rev. **105**, 1740 (1954).

$CoFe_2O_4$ are "inversed" spinels. $MgFe_2O_4$ and $MnFe_2O_4$ are intermediate cases, on which firing conditions and cooling have great influence.[17] The spectra show that, in the inversed structure, additional charge in the tetrahedral site increases the energy and restoring force associated with the bonds between the tetrahedral atom and its oxygen neighbors. This increases the frequency separation of ν_1 and ν_2 by 30 to 40 wave numbers. In addition, slight changes are expected because of the lowering of symmetry, but the large experimental band widths limit the sensitivity of this method of analysis.

An attempt was made to map the complete dispersion and absorption characteristics of nickel ferrite in the infrared, by measuring the polarization of the reflected light as a function of the angle of incidence on a single-crystal specimen. Unfortunately, the accuracy in this long wavelength range proved insufficient for reliable tracing of such curves. As a significant result, a value of κ', 7.0 ± 0.5, was obtained at the high-frequency side of the absorption ($\lambda\simeq5\ \mu$), as mentioned above. Since the value of κ' is of the order of 10 to 15 in the microwave region, the atomic polarization adds about 3 to 8 to the dielectric constant.

(c) Relaxation Spectra Caused by Interfacial Polarization[18]

While the dielectric constant of ferrites in the microwave range is only about 10 to 15, it may rise to values of 10^4 and higher as low frequencies are approached (Fig. 4.1). This behavior is typical for conducting materials through which the free flow of current is impeded, for example, by grain boundaries and barrier layers. A well-known prototype for a simple analysis of such effects is the Maxwell-Wagner two-layer capacitor (Fig. 5.5). Here the dielectric consists of two parallel sheets of materials (1) and (2), characterized by dielectric constant, conductivity and thickness. The apparent dielectric constant κ^* of the composite material, obtained by interpreting the admittance of the capacitor as

$$Y_{cap}=j\omega C=j\omega\kappa^* C_0 \tag{5.2}$$

is given by

$$\kappa^*=\kappa_\infty'+\frac{\kappa_s'-\kappa_\infty'}{1+j\omega\tau}-j\frac{\sigma}{\omega\epsilon_0}, \tag{5.3}$$

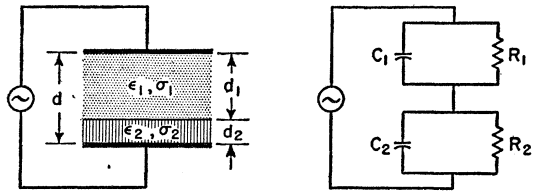

FIG. 5.5. Maxwell-Wagner two-layer capacitor and its equivalent circuit.

[17] G. Economos, J. Am. Ceram. Soc. **38**, 282, 335 (1955).
[18] See reference 5, pp. 228 ff.

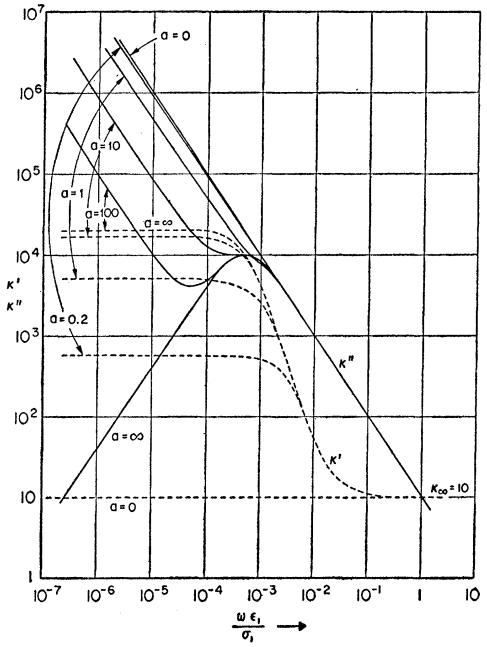

FIG. 5.6. Dielectric spectra of interfacial polarization.

where

$$\kappa_\infty'=\frac{(d_1+d_2)\epsilon_1\epsilon_2}{(d_1\epsilon_2+d_2\epsilon_1)\epsilon_0},$$

$$\kappa_s'=\frac{(d_1+d_2)}{\epsilon_0}\cdot\frac{(\epsilon_1 d_1\sigma_2^2+\epsilon_2 d_2\sigma_1^2)}{(\sigma_1 d_2+\sigma_2 d_1)^2},$$

$$\sigma=\frac{(d_1+d_2)\sigma_1\sigma_2}{(d_1\sigma_2+d_2\sigma_1)},$$

and

$$\tau=\frac{\epsilon_1 d_2+\epsilon_2 d_1}{\sigma_1 d_2+\sigma_2 d_1}.$$

Examination of (5.3) shows that the dispersion caused by the double layer is identical with that of the dipole relaxation of (4.4), while the absorption contains an additional term, $\sigma/\omega\epsilon_0$, dominant at low frequencies, due to the series resistors R_1 and R_2. In order to see the dependence of the dispersion and absorption characteristics on the relative properties of the two layers, we introduce factors of proportionality a and b, where

$$a=\frac{R_2}{R_1}=\frac{\sigma_1 d_2}{\sigma_2 d_1},\qquad b=\frac{C_2}{C_1}=\frac{\epsilon_2 d_1}{\epsilon_1 d_2}. \tag{5.4}$$

Figure 5.6 shows typical characteristics with the factor b chosen arbitrarily as 2000 and κ_∞' as 10, orders of magnitude frequently observed. The effect of increasing resistance ratios is illustrated by the parameter a.

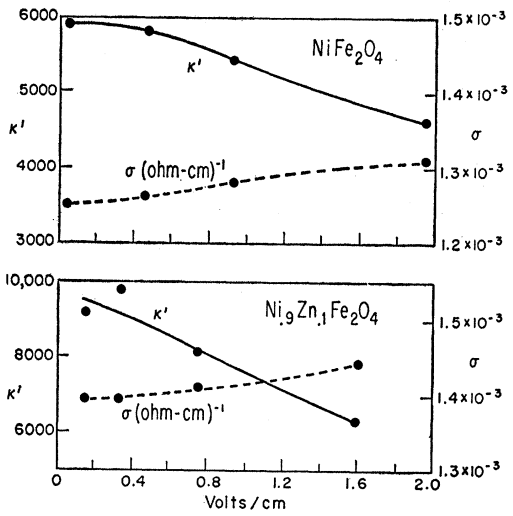

FIG. 5.7. Field-strength dependence of the interfacial polarization at 10^4 cps.

The two-layer model can be altered into an n-layer model of two media or into a dispersion of spherical particles of medium 1, distributed in a matrix of medium 2. As long as the relative amounts of media 1 and 2 remain the same, the complex permittivity stays unaltered. However, the prerequisite "spherical" is needed in order to preserve a simple relaxation spectrum with only one time constant.

Returning with this information to the electrical spectra of ferrites, we find, as did Koops,[19] that we can approximately match the observed characteristics (Figs. 7.1 and 7.2) by the equivalent circuit of Fig. 5.6 by choosing, for (5.4), parameter a between 0.1 and 1.5 and parameter b between 10^4 and 2×10^5. The ferrite proper (medium 1) is assumed to be dispersed as spherical particles in an interface (medium 2) which forms thin layers of high resistivity around the particles; hence $C_2 \gg C_1$, $R_2 \simeq R_1$, $\tau_2 \gg \tau_1$. In consequence, $b \gg 1$, $a \simeq 1$, and at sufficiently high frequencies the interface medium is shortened out, and one observes the dielectric properties of the base material.

For magnesium ferrite-aluminates a comparison with the two-layer model has been made by Fairweather and Frost[20]; constants a and b were derived from 2-terminal measurements. We find that 2-terminal data can be quite unreliable in the lower frequency range and may show a field-strength dependence which varies with the type of electrode used. Four-terminal measurements eliminate these difficulties. The remaining consistent field-strength dependence (Fig. 5.7) is probably caused by the high electric stress across the thin layers of medium 2, which leads to localized field emission and breakdown.

[19] C. G. Koops, Phys. Rev. **83**, 121 (1951).
[20] A. Fairweather and E. J. Frost, Proc. Inst. Elec. Engrs. **100**, Pt. IIA, 15 (1953).

(d) Spectra of Ionic Atmospheres

After the relaxation spectrum of the interfacial polarization has been traversed toward increasing frequency we should expect a characteristic which remains constant until the infrared absorption becomes noticeable. Instead, the dielectric conductivity begins to rise again appreciably between 10^9 and 10^{11} cycles (Fig. 5.8). A similar behavior is observed for glasses when they contain loosely bound cations (Fig. 5.9). Furthermore we find that while the microwave conductivity of a typical nickel-zinc ferrite increases slowly with temperature, the dc conductivity shows the exponential decrease expected for a normal semiconductor (Fig. 5.10).

This indicates that an additional absorption spectrum, lying in the 10^{11} to 10^{12} cps range, moves towards lower frequencies as the temperature decreases. Only the flat region of the σ characteristic is therefore descriptive of the electronic conductivity of the ferrites, while the bulk of the electric losses at micro-

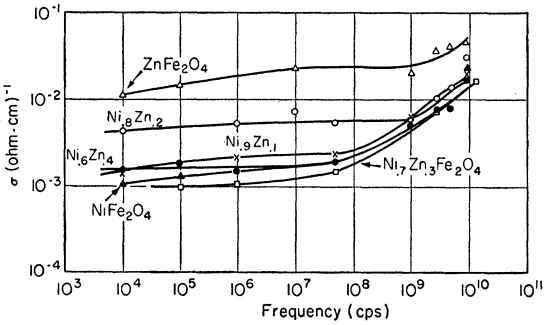

FIG. 5.8. Increase of the dielectric conductivity of ferrites towards the microwave region.

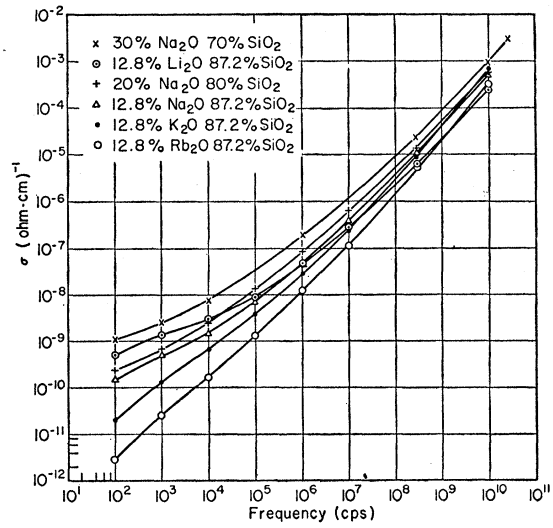

FIG. 5.9. Increase of the dielectric conductivity of glasses towards the microwave region.

wave frequencies arises from the incoming absorption spectrum.

This absorption is possibly caused by loosely bound charge carriers moving out of phase with their compensating ionic surroundings. Such spectra would be akin to the relaxation spectra of ionic atmospheres in liquids[21] (Wien effect), but might have resonance character in solids.

(e) The Conductivity of Ferrites

Interfacial polarization effects of ferrite ceramics certify that the observed conductivity may not at all be the true conductivity of the base material. There may be a variety of such effects, depending on composition and pre-treatment. For highly resistive ferrites, for example, an exponential increase of the conductivity with temperature has been reported to be governed by the same activation energy below and above the relaxation region.[20] In this case, the transition layers appear to be not of different electric properties but rather to be represented by geometrical intergranular contact areas. On the other hand, true transition layers frequently exist and can be identified, e.g., as a highly resistive surface layer of different texture (Fig. 5.11) in a sintered manganese-zinc sample.

Our research samples are, in general, fired to appreciably higher density (95–99% of x-ray density) than commerical samples (75–85%). In the case of our nickel-zinc ferrites this resulted in an increase in conductivity by about three orders of magnitude, even in the microwave region. The reason is probably that at high temperatures electron transitions take place from O^{2-} to Fe^{3+}. An excess of Fe^{2+} is created and the over-all charge balance restored by oxygen loss from the material. In cooling, a porous sample can reabsorb oxygen with relative ease from the firing atmosphere, and return to a low-temperature ferric equilibrium. For dense samples, the diffusion of the oxygen is too slow and a greater excess of ferrous iron remains.

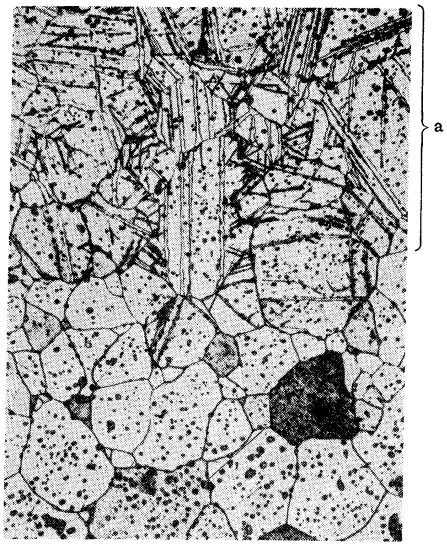

FIG. 5.11. Highly resistive surface layer (a) of manganese-zinc ferrite.

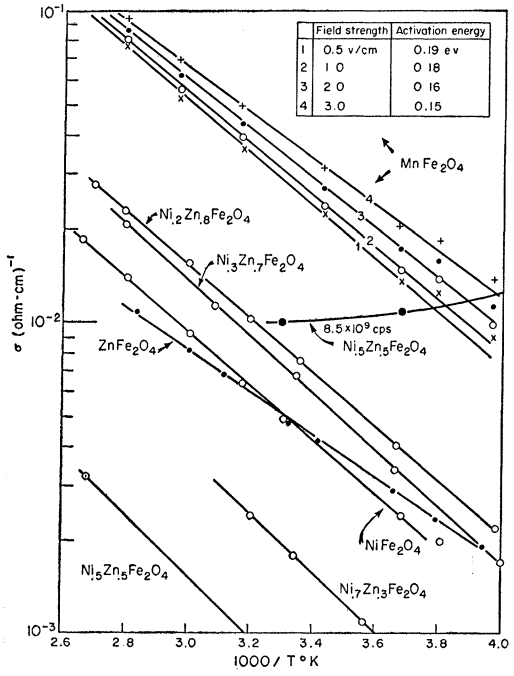

FIG. 5.10. Temperature dependence of the dc conductivity of ferrites (Epstein[45]).

This explanation is consistent with a number of other observations. Kamiyoshi[22] found that the activation energies of nickel ferrite and cobalt ferrite can be decreased considerably by quenching from high temperature. Wijn[23] showed that oxygen deficiency in a Ni-Zn ferrite can increase its conductivity from 10^{-6} to 10^{-3} (ohm cm)$^{-1}$ and lower the activation energy from 0.4 to 0.1 ev. Finally, measurements on single crystals of magnetite[24] have given us detailed information on the dominant role played by the $Fe^{2+} \rightarrow Fe^{3+}$ electron exchange in the conduction process.

The temperature dependence of the dc conductivity of a magnetite single crystal shows a very unusual characteristic (Fig. 5.12). One striking feature is an abrupt drop of the conductivity, by several orders of magnitude, when the crystal is cooled through a transition from cubic to orthorhombic symmetry near 119°K. This effect was interpreted by Verwey and co-workers[10] as an electronic order-disorder transition in the Fe^{2+}—Fe^{3+} occupation of the octahedral cation

[21] P. Debye and H. Falkenhagen, Physik. Z. **29**, 121 (1928); M. Wien and co-workers, Physik. Z. **37**, 155 (1936).

[22] K. Kamiyoshi, Sci. Repts. Research Inst. Tôhoku Univ. **3**, 716 (1951).

[23] H. P. J. Wijn, Lab. Philips Gloeilampenfabrieken, Separaat 2092, 1953.

[24] C. A. Domenicali, Phys. Rev. **78**, 458 (1950); B. A. Calhoun, *ibid.* **94**, 1577 (1954).

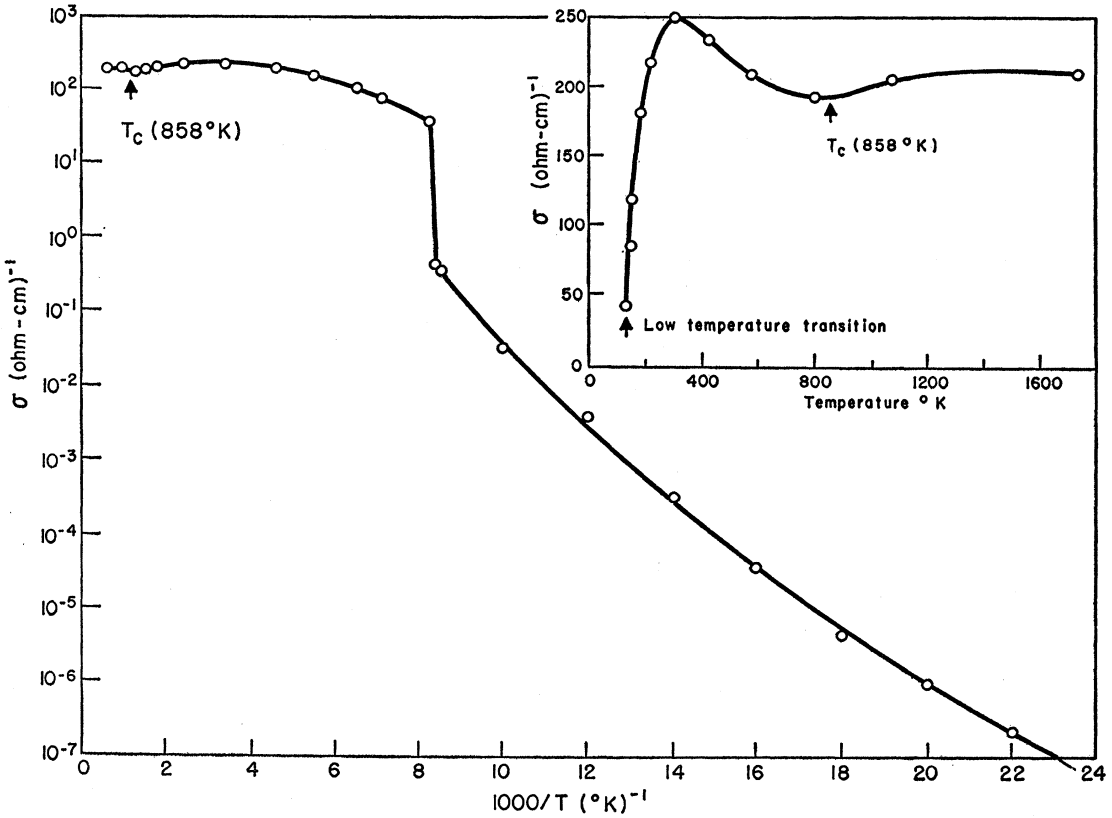

FIG. 5.12. Temperature dependence on the dc conductivity of the magnetite single crystal.

sites. Observations on a concurrent ordering of the magnetic spin system[24] support this explanation. The sharpness of the transition is rapidly destroyed by addition agents which interrupt the ferrous-ferric sequence in the octahedral sites (Fig. 5.13).

Without doubt the very high conductivity of magnetite is caused by the easy electron transfer in the octahedral sites, and the highly resistive ferrites are made by interrupting this transfer. The electron exchange in magnetite may be considered as an activation process, in which the electrons are handed along so fast above the transition that the vibrations cannot follow. At the transition, the lattice vibrations catch up and differentiate between ionic arrangements by different distortion of the structure at the Fe^{2+} and Fe^{3+} sites. Thus, above the transition only the electronic polarization enters into the activation process; below it, both the electronic and atomic polarization are involved. The ordering is not complete immediately below the transition, as conduction measurements show,[24] but improves with falling temperature; also the apparent activation energy, as measured by the slope of log conductivity *vs* $1/T$ curve, decreases slowly from 0.1 ev and reaches 0.03 ev at 40°K.

It is tempting to speculate that in magnetite single crystals the unusual case of band-type conduction in specific lattice directions [110] is realized, which changes below a critical temperature to a more classical trapping and release process. More research is needed to clarify this issue. At higher temperature, scattering by lattice vibrations flattens the slope of the conductivity characteristic and reverses it near 355°K. The new rise above the Curie point may be caused by strong onset of the higher energy electron transfer processes between O^{2-} and the cations postulated above. Such a transfer would simultaneously weaken the superexchange coupling causing ferromagnetism and be a determining factor for the Curie temperature. Electron transfer between cations on tetrahedral and octahedral sites may also become of importance in the disordered magnetic state.

6. MAGNETIC SPECTRA (GENERAL DISCUSSION)

(a) Gyroscopic Effects

The elementary magnetic moments $\mathbf{m}$ of a material are casually related to quantized angular momenta $\mathbf{p}'$ as

$$\mathbf{m}=\gamma\mathbf{p}', \tag{6.1}$$

where γ is the gyromagnetic ratio. Viewed classically, they are gyroscopes, subjected in a magnetic field $\mathbf{H}$, according to Newton's law, to a torque

$$\mathbf{T}=\frac{d\mathbf{p}'}{dt}=\mathbf{m}\times\mu_0\mathbf{H}, \tag{6.2}$$

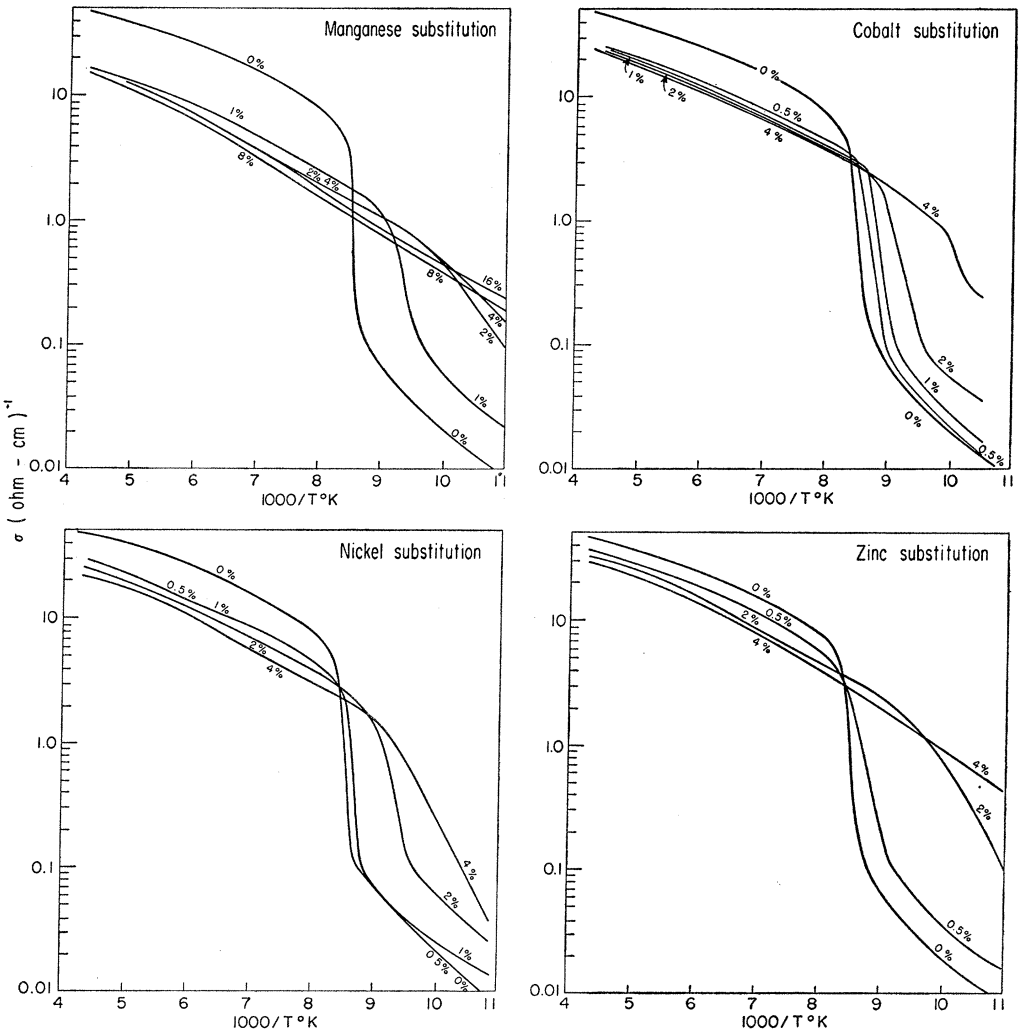

FIG. 5.13. Effect of cation substitution on the electronic order-disorder transition in magnetite (J. H. Epstein, M. S. thesis, Massachusetts Institute of Technology, 1954).

which causes a temporal change of the magnetic moment

$$\frac{d\mathbf{m}}{dt}=\gamma[\mathbf{m}\times\mu_0\mathbf{H}]. \tag{6.3}$$

The magnetization, represented by the additive action of N dipole moments per unit volume,

$$\mathbf{M}=N\mathbf{m}, \tag{6.4}$$

therefore obeys the equation of motion

$$\frac{d\mathbf{M}}{dt}=\gamma[\mathbf{M}\times\mu_0\mathbf{H}]. \tag{6.5}$$

Precession in Static Fields

If $\mathbf{H}$ represents a static field applied in the $+z$ direction,

$$|\mathbf{H}|=H_z=\text{constant}, \tag{6.6}$$

(6.5) has the solution

$$\begin{aligned} M_x&=M_0e^{j\omega_0t}\\ M_y&=M_0e^{(j\omega_0t+\pi/2)}\\ M_z&=\text{constant}=(M^2-M_0^2)^{\frac{1}{2}}, \end{aligned} \tag{6.7}$$

with $\omega_0=-\gamma\mu_0H_z$. The two oscillating components are out of phase by 90° in space and time, hence add up to a circular rotation in the x-y plane. The magnetization vector $\mathbf{M}$ precesses around the magnetic field axis. (The sign of ω_0 indicates a counterclockwise precession for $\gamma>0$, as viewed looking along the direction of the applied field.)

Superposition of a Small Alternating Magnetic Field

If the magnetization vector $\mathbf{M}$ is initially at rest, pointing in the direction of the static field H_z, the super-

position of a small alternating magnetic field

$$\Delta\mathbf{H}=(\Delta\mathbf{H})_0 e^{j\omega t} \tag{6.8}$$

again causes a precession. Without attenuation and by including only first-order terms, the torque equation (6.5) reads

$$\begin{aligned}\frac{d(\Delta M_x)}{dt}&=\gamma\mu_0[(\Delta M_y)H_z-M_z(\Delta H_y)]\\ \frac{d(\Delta M_y)}{dt}&=\gamma\mu_0[M_z(\Delta H_x)-(\Delta M_x)H_z]\\ \frac{d(\Delta M_z)}{dt}&=0,\end{aligned} \tag{6.9}$$

the solution of which is

$$\begin{aligned}\Delta M_x&\equiv a(\Delta H_x)-j\frac{\omega}{\omega_0}a(\Delta H_y);\\ \Delta M_z&\equiv a(\Delta H_y)+j\frac{\omega}{\omega_0}a(\Delta H_x),\end{aligned} \tag{6.10}$$

with

$$a\equiv\frac{\dfrac{M_z}{\omega_0^2}}{\omega_0^2-\omega^2}.$$

Expressing the relation between the magnetization and field components by a susceptibility matrix for the magnetic susceptibility χ_m*, we obtain $\chi_{11}=\chi_{22}=a$, and $\chi_{12}=-\chi_{21}=-j(\omega/\omega_0)a$,

$$\chi_m=\begin{Vmatrix} a & -j\dfrac{\omega}{\omega_0}a & 0\\ j\dfrac{\omega}{\omega_0}a & a & 0\\ 0 & 0 & 0\end{Vmatrix}. \tag{6.11}$$

An experiment designed to measure the diagonal susceptibilities χ_{nn} would therefore trace out the dispersion curve

$$\frac{\chi_{11}}{\chi_s}=\frac{\chi_{22}}{\chi_s}=\frac{\omega_0^2}{\omega_0^2-\omega^2}, \tag{6.12}$$

a resonance curve identical with that for an undamped linear oscillator (Sec. 4).

(b) Spin Resonance and Effective Field

In Eq. (6.7) we assumed that the Larmor frequency is determined by the applied field H_z; this is true only in isotropic magnetic media without domain and crystal boundaries. More generally, the resonance frequency can be represented as proportional to an "effective" field, $\mathbf{H}_{\text{eff}}$, which contains all influences that lead to a change in the free energy $\mathcal{E}$ of the magnetic system, when the magnetization vector $\mathbf{M}$ is turned from its equilibrium direction.[25] Writing the free energy $\mathcal{E}$ as a function of the polar angles θ and ϕ,

$$\begin{aligned}\omega_0&=-\frac{\gamma\mu_0}{M\sin\theta}\left[\frac{\partial^2\mathcal{E}}{\partial\theta^2}\cdot\frac{\partial^2\mathcal{E}}{\partial\phi^2}-\left(\frac{\partial^2\mathcal{E}}{\partial\theta\cdot\partial\phi}\right)^2\right]^{\frac{1}{2}}\\ &=-\gamma\mu_0 H_{\text{eff}}.\end{aligned} \tag{6.13}$$

The most important contributions of the material to the effective field are the following.

Magnetic Anisotropy of the Crystal Structure

In a crystal of cubic symmetry, for example, the anisotropy energy of the magnetization $\mathbf{M}$ can be expressed as

$$\begin{aligned}\mathcal{E}_a=K_0+K_1(\alpha_1^2\alpha_2^2+\alpha_2^2\alpha_3^2+\alpha_3^2\alpha_1^2)\\ +K_2(\alpha_1^2\alpha_2^2\alpha_3^2)+\cdots,\end{aligned} \tag{6.14}$$

where α_1, α_2, α_3 are the direction cosines of the magnetization vector in respect to the crystal axes (Fig. 6.1). Landau and Lifshitz[26] first pointed out that this anisotropy leads to an effective field, which for a single-domain crystal of spherical shape, when the first-order term dominates,[27] amounts to

$$H_{\text{eff}}=\frac{2K_1}{\mu_0 M_s}$$

for K_1 positive (easy direction [100])

and (6.15)

$$H_{\text{eff}}=-\frac{3K_1}{2\mu_0 M_s}$$

for K_1 negative (easy direction [111]).

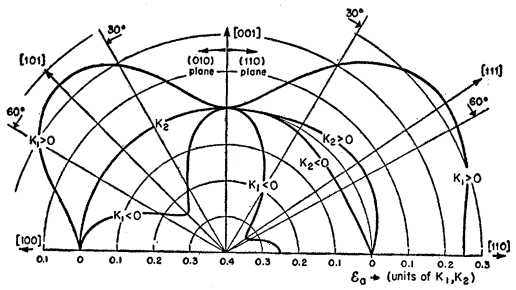

FIG. 6.1. Magnetic anisotropy energy in two planes of a cubic crystal.

[25] H. Suhl, Phys. Rev. **97**, 555 (1955).
[26] L. Landau and E. Lifshitz, Physik. Z. Sowjetunion **8**, 135 (1931).
[27] C. Kittel, Phys. Rev. **73**, 155 (1948).

Shape Factor

For ellipsoids the position of minimum energy for an isotropic ferromagnetic is the direction of the long axis, because the smallest demagnetizing field results (1.18). Hence, deflection of the magnetization vector from this direction gives rise to a torque tending to restore the minimum energy state. In this case the effective field for a single-domain ellipsoid[27] polarized in the z direction by a field H_z is given by

$$\mathbf{H}_{\text{eff}}=[H_z+(w_x-w_z)M_z]^{\frac{1}{2}}[H_z+(w_y-w_z)M_z]^{\frac{1}{2}} \equiv H_{x\text{eff}}{}^{\frac{1}{2}}H_{y\text{eff}}{}^{\frac{1}{2}}. \quad (6.16)$$

The maximum value is reached for a long needle ($w_x=w_y=\frac{1}{2}$, $w_z=0$)

$$H_{\text{eff}}=H_z+\tfrac{1}{2}M_s.$$

Induced Moments on Domain Boundaries

As the Curie point of a ferromagnetic is approached from higher temperature, the elementary spins spontaneously align and a saturation magnetization $\mathbf{M}$ develops in a preferred crystallographic direction. Several equivalent lattice directions are available and are usually chosen by the magnetic axes to produce a domain pattern approaching a constellation of minimum free energy.

A large "dynamic" effective field may be produced, as Polder and Smit showed,[28] because of the presence of domain boundaries. Figure 6.2 shows a section through a ferromagnetic body containing 180° domains orientated in the $\pm z$ direction with thin walls in the y-z planes. Application of an oscillatory field in the $\pm x$ direction, that is, perpendicular to the wall, produces a Larmor precession around the H_z field with the sense of rotation opposite in the up-and-down domains. In consequence, the poles in the x direction at the walls appear in phase and, adding to dipole chains, produce the normal shape magnetization factor w_x of the overall body. The poles created in the y direction are in opposition and their demagnetizing effect cancels ($w_{x,\text{eff}}=w_x$, $w_{y,\text{eff}}=0$, $w_z=0$).

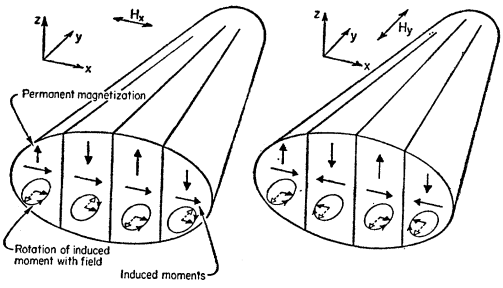

FIG. 6.2. Gyromagnetic rotation creating free poles on domain walls.

[28] D. Polder and J. Smit, Revs. Modern Phys. **25**, 89 (1953).

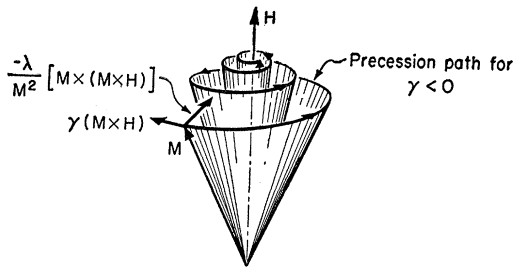

FIG. 6.3. Erecting torque damping gyromagnetic precession.

On the other hand, if the oscillatory field stands in the $\pm y$ direction, the free poles induced on the domain walls pile up in alternating sheets and lead to very strong closing fields in the individual domains ($w_{x\text{eff}}=1$; $w_{y\text{eff}}=w_y$; $w_z=0$). Since the shape factor in the x or y direction can vary between 0 and 1, the effective field for the first mode of excitation can vary between H_z and $H_z{}^{\frac{1}{2}}(H_z+M_z)^{\frac{1}{2}}$, and for the second mode, between $H_z{}^{\frac{1}{2}}(H_z+M_z)^{\frac{1}{2}}$ and (H_z+M_z).

The field action of induced moments invoked by Polder and Smit can be generalized; a system of n types of interacting domains will have n-resonant frequencies as do n-coupled oscillators. A complex domain arrangement pointing at various angles to the applied oscillatory field should therefore produce a broad distribution of Larmor frequencies whose effective fields lie for the most part in the range between the anisotropy field H_a and (H_a+M_z).

In addition to these resonances where the individual moments within each domain precess as a single spin system, the existence of magnetic sublattices in ferrites permits further modes of precession wherein the spin system of one sublattice changes its orientation with respect to the others.[29] The frequency of such modes should lie in the infrared region in most cases.[30] They have never been observed in simple ferrites. However, a resonance of this kind has been induced at microwave frequencies,[31] under the special condition that the sublattice moments were very nearly balanced.

Damping Effects

In real matter, the rotational energy of the Larmor precession will be dissipated by such effects as magnetic dipole radiation, interaction with nearby magnetic moments, with conduction electrons and, through magneto-elastic coupling with lattice vibrations. In consequence, the magnetization vector will spiral back into the z direction. This tendency can be expressed formally in the equations of motion by adding to the

[29] R. K. Wangsness, Phys. Rev. **91**, 1085 (1953); **93**, 68 (1954).

[30] J. Kaplan and C. Kittel, J. Chem. Phys. **21**, 760 (1953).

[31] R. K. Wangsness, Phys. Rev. **97**, 831 (1955); T. R. McGuire, *ibid.* **97**, 831 (1955).

rotational torque an erecting torque (Fig. 6.3)

$$\frac{d\mathbf{M}}{dt}=\gamma[\mathbf{M}\times\mu_0\mathbf{H}]-\frac{\lambda}{|\mathbf{M}|^2}[\mathbf{M}\times(\mathbf{M}\times\mathbf{H})] \equiv\gamma[\mathbf{M}\times\mu_0\mathbf{H}]+\lambda\left[\mathbf{H}-\frac{(\mathbf{M}\cdot\mathbf{H})\mathbf{M}}{|\mathbf{M}|^2}\right], \tag{6.17}$$

as first introduced by Landau and Lifshitz.[26] Up to the present, no theory has adequately explained why the attenuation is so strong in ferrites; the relaxation times are of the order of 10^{-9} sec. In considering this problem it is convenient to regard the precessional motion of the magnetization vector as a periodic disturbance of the system of spin moments, which leaves all these moments mutually parallel; that is, the wave motion in the spin system has an infinite wavelength or zero wave number $\mathbf{k}$. Disturbances of shorter wavelengths may also exist and would have the effect of reducing the over-all magnetic moment of the spin system. Only the wave with $\mathbf{k}=0$ can be excited by a uniform field. Since there is little interaction of this wave by magnetic-elastic coupling with the thermal vibrations of the lattice[32] (the bulk of which have wave numbers of the order of 10^9 m^{-1}), it has been difficult to explain the attenuation as a direct energy transfer process. It has been suggested[32] that energy is first transferred from the $\mathbf{k}=0$ wave to waves of higher $\mathbf{k}$ value and thence to the lattice, but this process itself has remained unexplained, since in a system of infinite extent much more energy is required to excite a wave of high $\mathbf{k}$. This is because, when neighboring spins are moved out of alignment, exchange energies enter of the form

$$\mathcal{E}_k=\gamma\mu_0 H\hbar+Xk^2, \tag{6.18}$$

where X is a constant of the order of 10^{-40} joule m^2.

Lately, it has been realized[33] that for a magnetic system of finite extent this energy expression has to be modified considerably. For example, a disturbance of large wave number in a sphere, oriented along the external field direction, induces alternate N and S poles on the surface of the sphere (Fig. 6.4), which, in contrast to the case of $\mathbf{k}=0$, effectively cancel each other's influence at a distance large to their separation. Therefore the precessing dipoles of this wave mode contribute magnetization components only in the z direction, hence the demagnetizing factors are $w_z=\frac{1}{3}$, $w_x=w_y=0$, and the energy of the wave is (Fig. 6.5)

$$\mathcal{E}_k=\hbar\gamma\mu_0\left(H_z-\frac{M}{3}\right)+Xk^2. \tag{6.19}$$

For wave propagation at an angle θ to the field axis in a spheroid

$$\mathcal{E}_k=[\hbar\gamma\mu_0(H_z-N_zM)+Xk^2]^{\frac{1}{2}} \times[\hbar\gamma\mu_0(H_z-N_zM+M\sin^2\theta)+Xk^2]^{\frac{1}{2}}. \tag{6.20}$$

For very low $\mathbf{k}$ values, the situation is more complicated and has been treated theoretically by Walker.[34] Such modes have been excited by nonuniform fields[35] (Fig. 6.6). It is clear from (6.20) and Fig. 6.5 that many modes with comparatively large $\mathbf{k}(\simeq 10^{7\to 8}[\mathrm{m}^{-1}])$ may have approximately the same energy as the $\mathbf{k}=0$ wave.

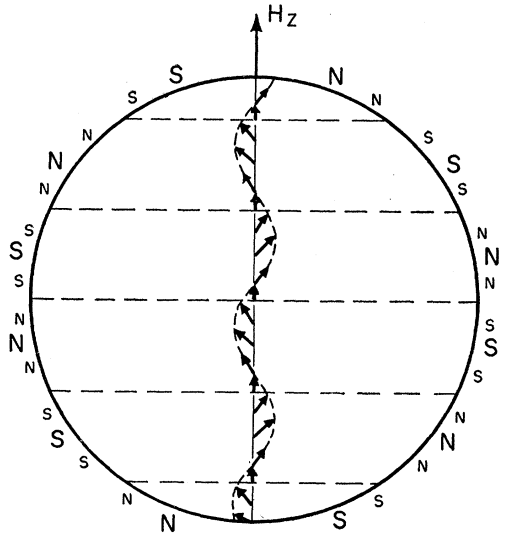

FIG. 6.4. Dynamic pole distribution on sphere caused by high-order spin wave.

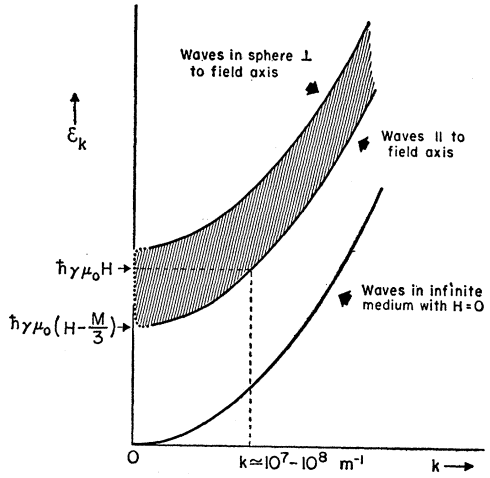

Fig. 6.5. Energy of spin waves propagating in sphere.

[32] C. Kittel and E. Abrahams, Revs. Modern Phys. **25**, 233 (1953).

[33] Clogston, Suhl, Walker, and Anderson, Phys. Rev. **101**, 903 (1956).

[34] L. R. Walker, Phys. Rev. **105**, 390 (1957).

[35] P. A. Miles, thesis, London, 1954 (unpublished); White, Solt, and Mercereau, Bull. Am. Phys. Soc. Ser. II, **1**, 12 (1956); J. F. Dillon, Jr., *ibid.* Ser. II, **1**, 125 (1956); R. L. White and I. H. Solt, Jr., Phys. Rev. **104**, 56 (1956).

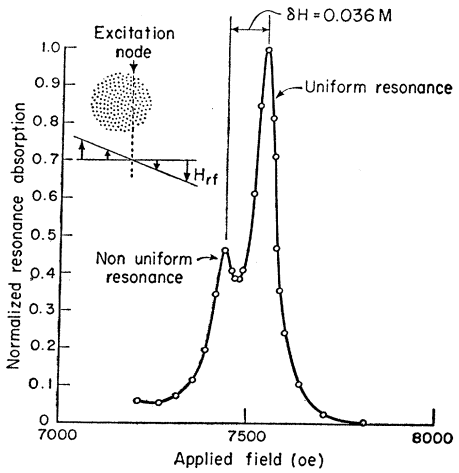

FIG. 6.6. Magnetic resonance doubling at 24 kmc in a nickel ferrite crystal sphere produced by nonuniform excitation (Miles[35]).

The fact that structural inhomogeneities in the lattice may provide coupling between these waves offers some hope for the explanation of resonance damping in ferrites.

The resonance frequency, hence energy, of the uniform mode depends on the shape of the specimen. It follows that the degree of degeneracy of the spin-wave system, and with it the resonance damping, may also be shape-dependent. Thus the damping for a rod magnetized along its axis should be more than for a sphere, because more spin-wave modes of approximately equal energy can be excited in the rod. Such effects have not yet been reported. The spin-wave theory predicts[36] in addition that the uniform precession mode, directly excited, may become unstable at large amplitudes of oscillation. The reduction of resonance absorption in metals and ferrites at high levels of rf excitation observed by Bloembergen and co-workers[37] is believed to be due to this instability.

We will use the Landau-Lifshitz formalism for the future discussion, despite the fact that the mechanism outlined above would not conserve the length of the vector **M**. The damping factor will therefore be considered as a parameter which may depend on both **H** and **M**.

The solution of (6.17) is

$$\begin{aligned} M_x &= M_0 e^{(j\omega_0-\alpha)t} \\ M_y &= M_0 e^{(j\omega_0-\alpha)t+\pi/2} \\ M_z &= M\left\{1-\left(\frac{M_0}{M}\right)^2 e^{-2\alpha t}\right\}, \end{aligned} \tag{6.21}$$

with $\alpha=(\lambda H/M)$. By introducing the erecting torque, the oscillators in the x-y plane remain out of phase by 90° in space and time but are attenuated. The resonance frequency ω_0 is still identical to the Larmor frequency of (6.7).

Corresponding to (6.10), which relate to the application of a small oscillatory field, we now have

$$\begin{aligned} \Delta M_x &= a'(\Delta H_x) - jb'(\Delta H_y) \\ \Delta M_y &= a'(\Delta H_y) + jb'(\Delta H_x), \\ \Delta M_z &= 0 \end{aligned} \tag{6.22}$$

where

$$a' \equiv \frac{\omega_0\omega' + \lambda\alpha + j\omega\lambda}{\omega_0^2 + (j\omega+\alpha)^2}, \quad b' \equiv \frac{\omega\omega'}{\omega_0^2+(j\omega+\alpha)^2}$$

and $\omega' = -\gamma\mu_0 M_z$.

For very low frequencies in relation to ω_0, the $\Delta\mathbf{M}$ vector in the plane oscillates practically in the direction of and in phase with the driving field; for very high frequencies ($\omega \gg \omega_0$), the magnetization vector is essentially out of phase by 90° in space and 180° in time; at the Larmor frequency itself, the $\Delta\mathbf{M}$ vector describes a circular motion in the x-y plane (Fig. 6.7) with a temporal phase shift of 90° with respect to the driving field ΔH. Energy is continuously absorbed from the exciting field and transferred to the surrounding medium via the damping process.

In comparison with the case of undamped motion (6.12), the diagonal susceptibility terms now have the form

$$\frac{\chi_m^*}{\chi_{ms}'} = \frac{\omega_0^2+\alpha^2+j\omega\alpha}{\omega_0^2+\alpha^2-\omega^2+j\omega 2\alpha}. \tag{6.23}$$

The dispersion and absorption curves for this resonance response are very similar to those of Figs. 4.2 and 4.4 for low damping, where the line width $\Delta\omega = 2\alpha$, but deviations occur at low Q values (Fig. 6.8). In the limit for extreme damping ($\lambda \gg -\gamma\mu_0 M$), the response follows a simple relaxation curve, but this time the loss maximum shifts to a frequency $\omega = (1/\tau) = (\lambda H/M)$ much higher than the resonance frequency ω_0. Physically this means that if the system is perturbed, equilibrium is regained so rapidly that the precession is unable to take place.

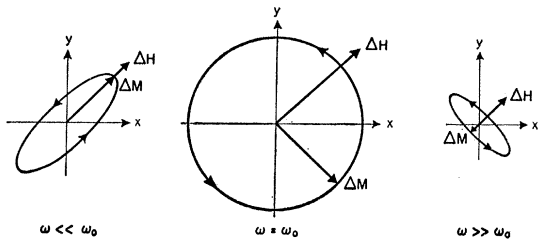

FIG. 6.7. Equilibrium precession of magnetization vector in small oscillatory field.

[36] P. W. Anderson and H. Suhl, Phys. Rev. **100**, 1788 (1955).
[37] N. Bloembergen and S. Wang, Phys. Rev. **93**, 72 (1954); R. W. Damon, Revs. Modern Phys. **25**, 239 (1953).

If the factor λ is a physical constant of the material, the Q value of the resonance is independent of the frequency, since

$$Q=\frac{\omega_0}{2\alpha}=-\frac{\gamma\mu_0 H_{\rm res}}{2\lambda H_{\rm res}}\cdot M=-\frac{\gamma\mu_0 M}{2\lambda}. \quad (6.24)$$

Thus if the resonance is traced by varying the applied field $\mathbf{H}$ at a fixed frequency ω, the resonance line width ΔH should be proportional to ω. In ferrite single crystals, line widths measured in the microwave region are found to vary linearly with ω, but not proportional to ω (Fig. 6.9). Thus, no unique frequency-independent constant λ can be used to describe such resonances in ferrites. In the frequency region 10^{10} to 4×10^{10} cps, at least, we can take care of this fact in a formal way by introducing a further damping factor δ in the form

$$\partial\mathbf{M}/\partial t=\gamma\mu_0(\mathbf{M}\times\mathbf{H}) -\left(\frac{\lambda}{M^2}+\frac{\delta}{MH}\right)(\mathbf{M}\times\mathbf{M}\times\mathbf{H}). \quad (6.25)$$

The attenuation factor α of (6.21) now becomes

$$\alpha=\frac{\lambda H}{M}+\delta \quad (6.26)$$

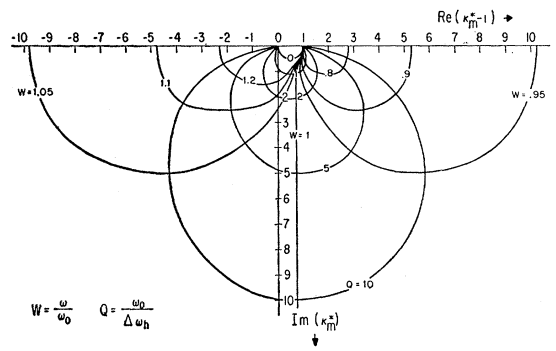

FIG. 6.8. Resonance response with Landau-Lifshitz damping.

with the contribution δ describing a frequency-independent line width. A damping process of this form gives an energy loss per cycle which depends solely on the deviation of the magnetization vector from its equilibrium position and not upon the static field applied. If the line widths found in nickel ferrite (see Fig. 6.9) are due to damping, the appropriate values of the constants are $\delta=3.2\times10^8$ rad/sec $\lambda=1.3\times10^8$ rad/sec.

(c) Domain Walls

Adjacent areas in a crystal, where the spin arrays are aligned along different axes of easy magnetization, are separated by transition regions (domain walls) in which the spins change direction gradually (Fig. 6.10).

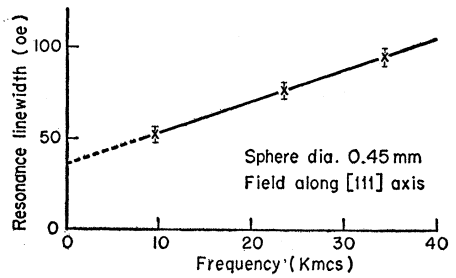

FIG. 6.9. Resonance line width of nickel ferrite single crystal at microwave frequencies (Miles[35]).

The precise structure of the wall is determined by a compromise between opposing forces of magnetocrystalline anisotropy trying to align all spins along the preferred axes (hence to minimize the thickness of the transition layer) and exchange energy, forcing spins into parallel alignment (hence expanding the wall in order to minimize the misalignment of neighboring spins). The resultant energy stored in a wall may be shown[21,38] to be proportional to the product $(AK_1)^{\frac{1}{2}}$, and its thickness of the order of $(A/K_1)^{\frac{1}{2}}$ where K_1 is the first-order anisotropy constant and A an exchange-energy factor usually of the order of 10^{-10} joule/m. Estimates of wall energies for known ferromagnetics lie in the range 10^{-4} to 10^{-2} joule/m^2 for walls of 10^2 to 10^4 angstroms thickness.

The motion of domain walls has been treated in the following way[26,39]: the application of an external field H_z produces a torque on the magnetic spins in the wall proportionally to sin θ. Since the spins behave as gyroscopes, there tends to develop a precession around the z axis carrying the spins out of the y-z planes. Because the spins are coupled and staggered, an actual precession cannot take place but a wall deformation results, producing a magnetization in the x direction. This component M_x creates a closing field

$$H_x=-M_x \quad (6.27)$$

because div $B_x=0$ (div B_y and div B_z are, *a priori*, zero for a wall of infinite sidewise extension). The torque exerted by H_z, and hence the wall distortion and the M_x components, are a maximum in the middle of the wall, where the closing field H_x may be appreciably larger than the applied field H_z.

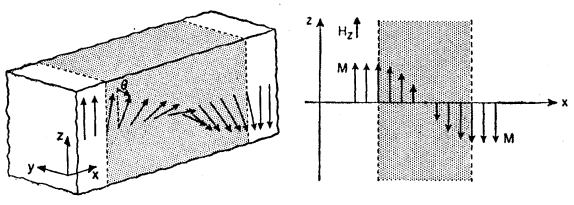

FIG. 6.10. Structure of 180° domain wall.

[38] C. Kittel, Revs. Modern Phys. **21**, 541 (1949).
[39] W. Döring, Z. Naturforsch. **3A**, 373 (1948); R. Becker, J. phys. radium **12**, 332 (1951); Rado, Wright, and Emerson, Phys. Rev. **80**, 273 (1950).

Due to the H_x field component, an additional precession motion about H_x ensues and this, coupled with the damping torques directed towards H_x and H_z (according to the Landau-Lifshitz expression) erects the moments into the z direction and causes the wall to move in the x direction. The wall structure is assumed to remain unchanged during translation, while the individual spins are left behind as particles in any wave motion. For the individual dipoles the instantaneous angular velocity for precession around the x axis is

$$\omega_0 \equiv \frac{d\theta}{dt} = -\gamma\mu_0 H_x, \tag{6.28}$$

and determines the translation velocity v (Fig. 6.10) as

$$\frac{d\theta}{dt} = \frac{d\theta}{dx} \cdot v; \tag{6.29}$$

hence

$$H_x = \frac{v}{\mu_0\gamma}\frac{d\theta}{dx}. \tag{6.30}$$

In moving the wall a unit distance, the potential energy of the system is reduced by the reversal from antiparallel to parallel of moment $2M$ per unit area of wall. The associated energy $2\mu_0 M H_z$ must be transferred to the lattice by the damping mechanism operating on the re-orientating dipole moments in the wall. According to (6.17), this mechanism gives a dissipation rate $\mu_0 H \cdot (dM/dt) \simeq \mu_0 \lambda H_x^2$, since for low damping $H_x \gg H_z$ in the center of the wall. The consequence of the introduction of the Landau-Lifshitz term is to give a rate of damping which increases with wall distortion, and hence with wall velocity.

The equilibrium velocity v is given by the balance of the rates of energy creation and dissipation

$$2MH_z\mu_0 v = \int_{-\infty}^{\infty} \mu_0 \lambda H_x^2 dx = \frac{v^2\lambda}{\gamma^2\mu_0}\int_{-\infty}^{\infty}\left(\frac{d\theta}{dx}\right)^2 dx,$$

whence

$$v = \frac{2\gamma^2\mu_0^2 M}{\lambda\int_{-\infty}^{\infty}\left(\frac{d\theta}{dx}\right)^2 dx} \cdot H_z = \frac{2\mu_0 M H_z}{\beta}. \tag{6.31}$$

The driving force per unit area $2\mu_0 M H_z$ is equal to the frictional damping force βv.

The wall distortion causing H_x also implies an increase in the energy stored in the wall structure. This additional deformation energy per unit area is

$$\Delta\mathcal{E}_w = -\frac{\mu_0}{2}\int_{-\infty}^{\infty} M_x H_x dx = \frac{\mu_0}{2}\int_{-\infty}^{\infty} H_x^2 dx = \frac{v^2}{2\gamma^2\mu_0}\int_{-\infty}^{\infty}\left(\frac{d\theta}{dx}\right)^2 dx. \tag{6.32}$$

The coefficient of $v^2/2$ may be interpreted as an effective wall mass

$$m = \frac{1}{\gamma^2\mu_0}\int_{-\infty}^{\infty}\left(\frac{d\theta}{dx}\right)^2 dx = \frac{\beta}{\lambda}. \tag{6.33}$$

This description of wall motion tacitly assumes that the equation of motion for individual spins can be handled as if all the magnetization vectors would execute their precession with equal amplitude and phase. Actually, the introduction of a wall distortion that moves past lattice imperfections suggests that exchange coupling effects may become of importance.[40] Furthermore, a wall region may differ in its properties from the bulk material (Sec. 7); hence damping processes effective in domain precession and domain-wall motion may not be identical.

When a wall is stabilized in position by the presence of impurities, cavities, stress patterns, etc., an elastic restoring force of the type $F_x = -kx$ exists for small displacements. Consequently, the equation of motion of the trapped wall may be written as that of an harmonic oscillator of the mass m subjected to frictional damping, i.e.,

$$m\ddot{x} + \beta\dot{x} + kx = 2\mu_0 M H_z. \tag{6.34}$$

If a periodic field $H_z = H_z e^{i\omega t}$ is applied, a susceptibility contribution stemming from the oscillating walls is observed,

$$\chi_{mz}^* \equiv \frac{\Delta M_z}{H_z} = \frac{2Mx}{H_z}n. \tag{6.35}$$

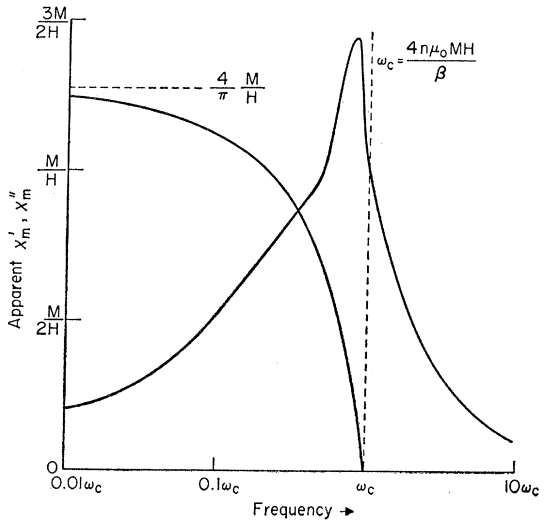

FIG. 6.11. Contribution to magnetic dispersion and loss by migrating domain walls (fundamental component derived from harmonic analysis).

[40] Exchange effects have been observed in a ferromagnetic resonance experiment in a metal, where a pronounced skin effect caused the exciting field, and with it the precession motion, to be rapidly attenuated with depth (W. S. Ament and G. T. Rado, Phys. Rev. **94**, 1411 (1954); **97**, 1558 (1954).

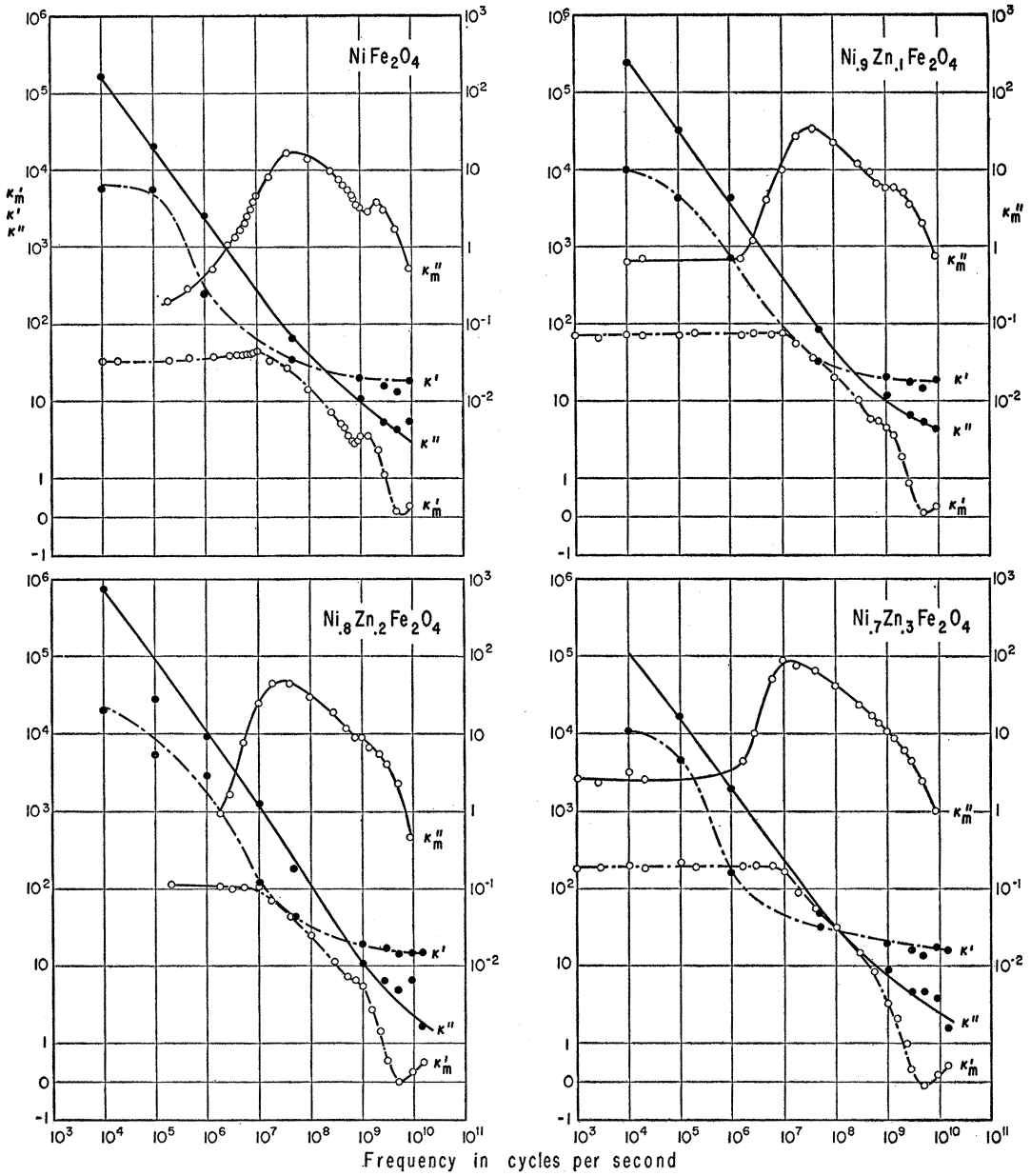

FIG. 7.1. Dielectric spectra of nickel-zinc ferrites from 10^3 to 10^{11} cps.

Here $2Mx$ represents the moment reversed for one wall displaced by x, and n the number of walls per unit length, in the x direction. Hence

$$\chi_{mz}^*=\frac{n4\mu_0M^2/m}{\omega_0^2-\omega^2+j\omega\lambda}, \tag{6.36}$$

with $\omega_0^2=k/m$. The ratio of dynamic to static susceptibility is therefore

$$\frac{\chi_{mz}^*}{\chi_{ms}}=\frac{\omega_0^2}{\omega_0^2-\omega^2+j\omega\lambda}=\frac{k}{k-m\omega^2+j\omega\beta} \tag{6.37}$$

where $\chi_{ms}=4n\mu_0M^2/k$. In the case of high damping ($\beta\gg m\omega$), this resonance response approaches a relaxation form

$$\frac{\chi_{mz}^*}{\chi_{ms}}\sim\frac{k}{k+j\omega\beta}=\frac{1}{1+j\omega\tau}, \tag{6.38}$$

with the relaxation time $\tau=(\beta/k)=(\lambda/\omega_0^2)$. If the walls are not bound to equilibrium positions but move through the crystal with a velocity given by (6.31), the susceptibility becomes

$$\chi_{mz}^*=-j\left(\frac{4n\mu_0M^2}{\beta\omega}\right), \tag{6.39}$$

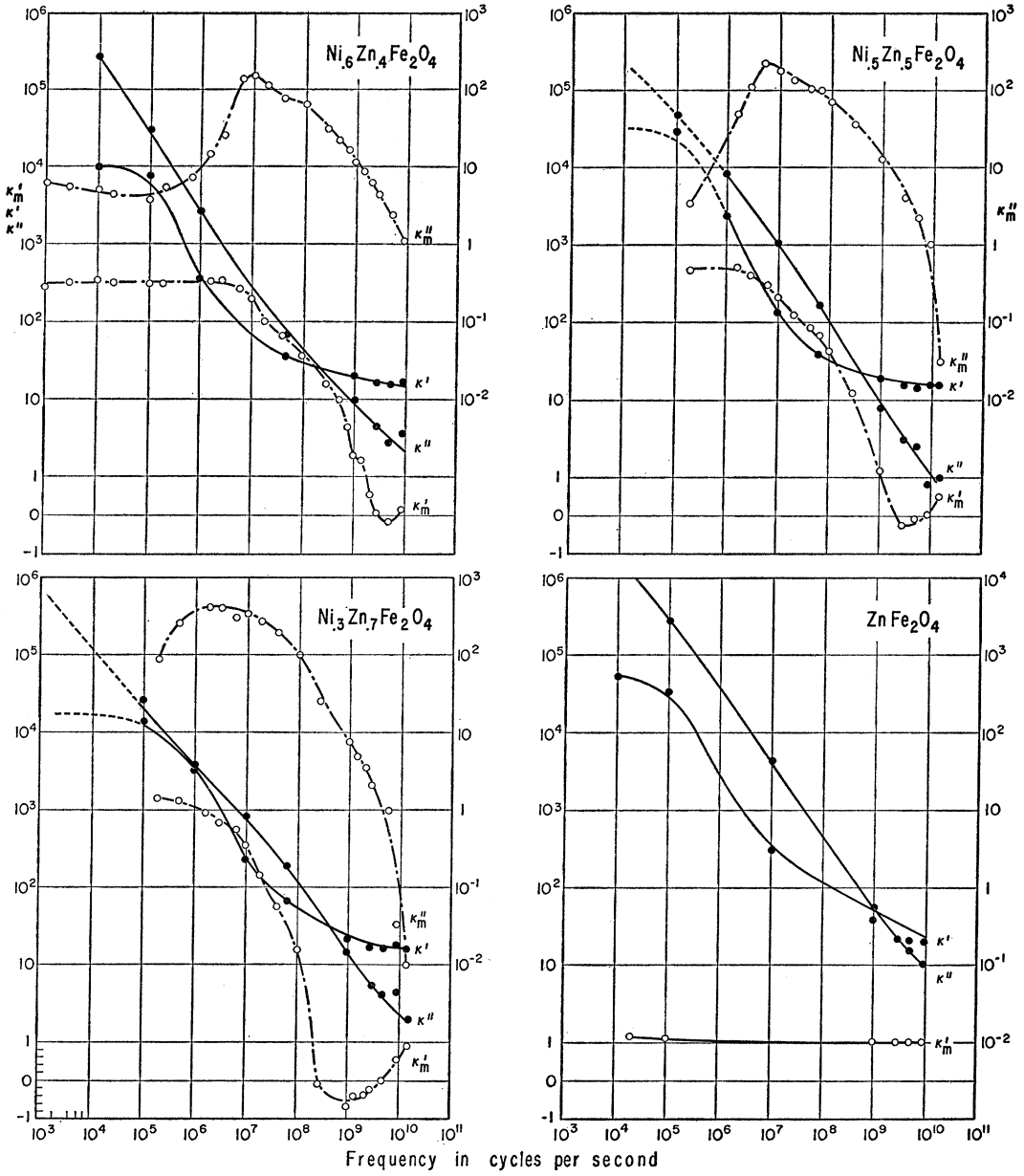

FIG. 7.2. Dielectric spectra of nickel-zinc ferrites from 10^3 to 10^{11} cps.

that is, a pure magnetic loss which varies with frequency in the same way as an electric loss due to charge migration. If this wall motion is interrupted at the critical frequency $\omega_c = 4\pi\mu_0 M H_z/\beta$ by the walls being swept out of the crystal, the magnetic response is no longer linear. The harmonic analysis of this new response at frequencies below ω_c has fundamental components both in and out of phase with the exciting field (Fig. 6.11). It can be seen that a distribution of critical frequencies can produce a dispersion spectrum similar to a relaxation, but this will be accompanied by an abnormally high and steep loss characteristic. The introduction of a finite coercive field H_c produces a nonlinear response at all frequencies and an additional frequency-dependent loss component below the appropriate critical frequency.

7. MAGNETIC SPECTRA OF FERRITES

The preceding discussion foresees three dispersion mechanisms: migration of domain walls, oscillation of domain walls around equilibrium positions, and gyromagnetic rotation of the magnetization vectors within domains. The migration of walls causes a loss similar to conduction phenomena, and possibly a relaxation-like spectrum; wall oscillation and gyromagnetic rotation, if not overdamped, produce resonance spectra.

Wall or Spin Resonance?

The frequency-response characteristics of the nickel-zinc ferrite series at room temperature (Figs. 7.1 and 7.2), as well as those of other ferrites, give the impression that there are two main dispersion regions showing some resonance character. The first is marked by a rapid increase in magnetic loss combined with a slight rise in the κ_m' characteristic in the range of 10^6 to 10^7 cps; the second by a loss peak and a minimum of κ_m' between 10^9 and 10^{10} cps. Rado and co-workers[41] advanced the interpretation that the upper and lower resonance regions are caused by spin and by domain-wall resonance, respectively, while scientists at the Philips Research Laboratories[42] are inclined to attribute both regions in cubic ferrites to spin resonance.

It cannot be postulated that the frequency location of the resonance region gives an *a priori* decision about the mechanism involved. The two main pieces of experimental evidence supplied by these characteristics are the static susceptibility χ_{ms} and the resonance frequency as identified by a loss maximum. These quantities are theoretically interrelated (Sec. 6).

For *wall resonance*, where $\omega_0=(k/m)^{\frac{1}{2}}$ and $\chi_{ms}=4C\mu_0M^2/k$ (6.36) with the factor C given by the number of walls and their relative orientation,

$$\omega_0^2\chi_{ms}=\frac{4C\mu_0M^2}{m}. \tag{7.1}$$

By introducing typical experimental values: $M=2.5\times10^5$ amp/m, $\chi_{ms}=30$, 10^4 walls per meter, and a wall mass as calculated for nickel ferrite (9×10^{-10} kg/m^2), we obtain a resonance frequency $\omega_0/2\pi=55$ Mc/sec. Over-damping of the wall leads to a loss-maximum frequency $\omega_d=(k/\lambda m)$ and

$$\omega_d\chi_{ms}=\frac{4C\mu_0M^2}{\lambda m}. \tag{7.2}$$

With a typical damping factor, taken (with the reservations discussed in Sec. 6b) from magnetic resonance data ($\lambda\simeq1\times10^9$ rad/sec), the loss-maximum frequency is lowered to $\omega_d/2\pi\simeq20$ Mc/sec.

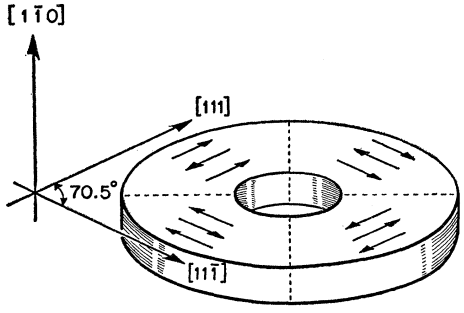

FIG. 7.3. Toroid of nickel ferrite single crystal cut in (110) plane.

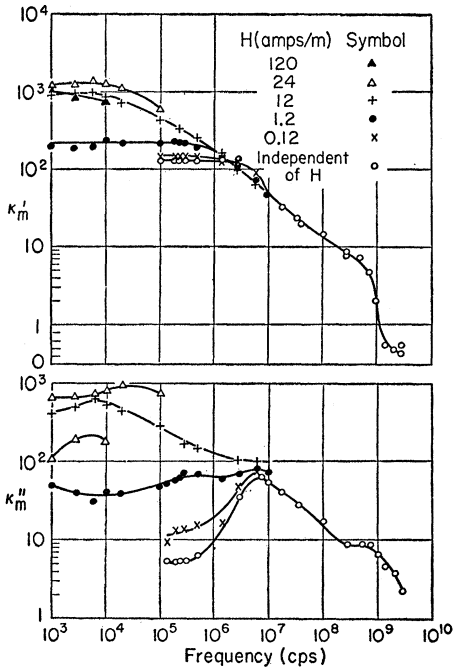

FIG. 7.4. Magnetic spectrum of nickel ferrite single crystal.

Deriving the corresponding relations for *spin resonance* requires knowledge of the effective (inner) field which acts on the spin system; it depends on anisotropy energy and on shape and domain-walls factor. If the inner field stands in the z direction ($H_{z\text{eff}}$), a small magnetic applied in the x or y direction may see different susceptibilities because the inner field does not necessarily have rotational symmetry (i.e., the restoring forces may be different in the two directions). Hence (6.16)

$$\chi_{(ms)x}=\frac{C'M}{H_{x\text{eff}}}$$

$$\chi_{(ms)y}=\frac{C'M}{H_{y\text{eff}}} \tag{7.3}$$

$$\omega_0=-\gamma\mu_0(H_{x\text{eff}}H_{y\text{eff}})^{\frac{1}{2}}.$$

Thus

$$\omega_0\chi_{(ms)x}=-\gamma\mu_0C'M\left(\frac{H_{y\text{eff}}}{H_{x\text{eff}}}\right)^{\frac{1}{2}}; \tag{7.4}$$

in the case of axial symmetry ($H_{x\text{eff}}=H_{y\text{eff}}$) the product is simplified to

$$\omega_0\chi_{ms}=-\gamma\mu_0C'M. \tag{7.5}$$

The factor C' takes account of the spatial distribution of the spin axes of the various domains. The experimental values given above, plus a random distribution for the various spin-axis directions ($C'=\frac{2}{3}$), lead to a Larmor frequency $\omega_0/2\pi=180$ Mc/sec. If the spin

[41] G. T. Rado, Revs. Modern Phys. **25**, 81 (1953).
[42] J. L. Snoek, Physica **14**, 207 (1948); D. Polder and J. Smit, Revs. Modern Phys. **25**, 89 (1953).

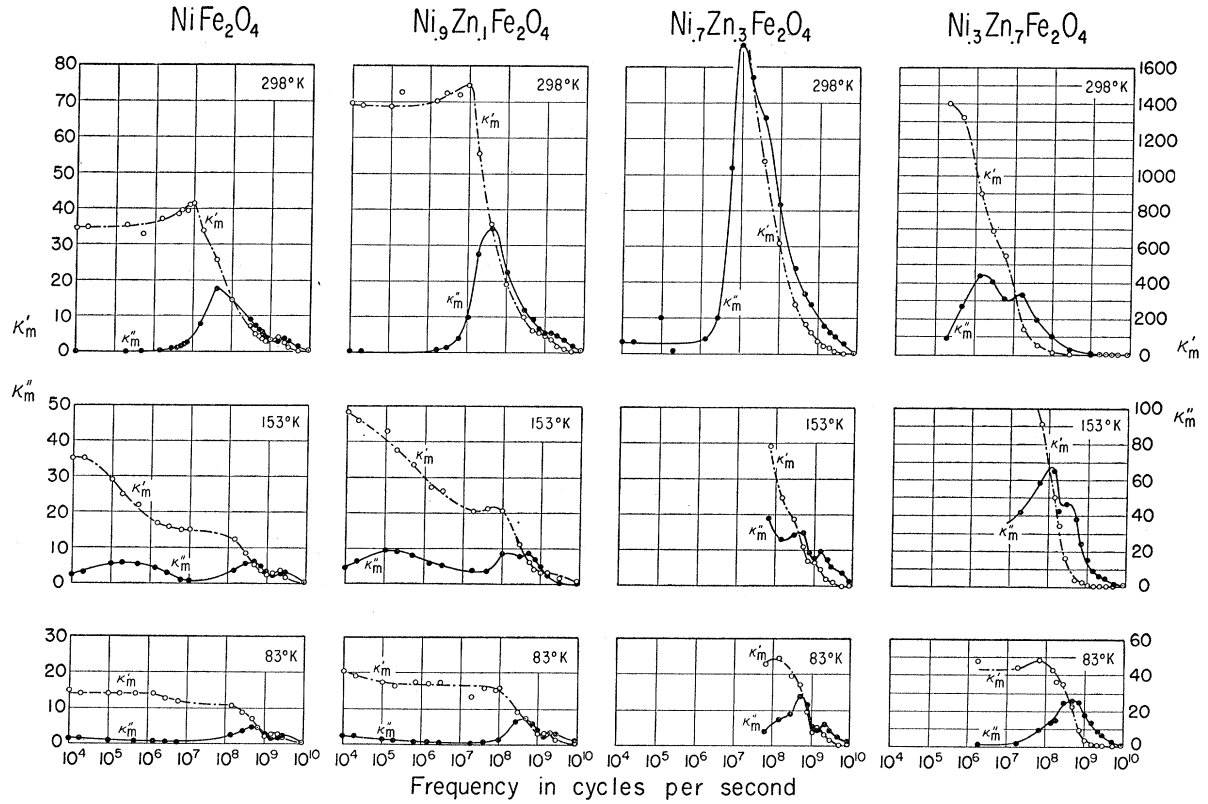

FIG. 7.5. Temperature dependence of magnetic spectra of nickel-zinc ferrite ceramics.

resonance becomes overdamped ($\lambda > |\gamma\mu_0 M|$), the loss maximum occurs at a frequency

$$\omega_d = \alpha = \frac{\lambda H_{\text{eff}}}{M}, \tag{7.6}$$

hence

$$\omega_d \chi_{ms} = C'\lambda. \tag{7.7}$$

However, with $\lambda = 1\times10^9$ rad/sec, as above, the dispersion would retain its resonance character and the loss-peak frequency would remain practically unchanged.

The domain-wall resonance in our example lies at a frequency somewhat lower than that of the spin resonance, but due to the arbitrary choice of the number of walls present, there is no clear order-of-magnitude distinction. When dealing with unknown domain arrays and multicrystalline structure of ceramics, the whole calculation rests on shaky grounds. Additional information can be provided by measurements on single crystals, by temperature- and field-strength effects and by a careful analysis of the influence of cation substitution.

Single-Crystal Measurements

The only single crystal available in the nickel-zinc ferrite series was a nickel-ferrite crystal grown by flame fusion.[43] It was cut in the shape of a toroid, oriented with a (110) plane parallel to the toroid plane (Fig. 7.3); the two [111] directions in this plane are directions of easy magnetization at room temperature. The cylindrical shape was a compromise between the ideal diamond shape with a simple domain pattern for quasi-static studies,[44] and the need to take measurements over a wide frequency range.

At low field strengths the frequency-response curve (Fig. 7.4) shows a general similarity to that of the ceramic, but the loss peaks are higher and more widely separated. It appears that there are two dispersion regions, centered near 8 and 600 Mc/sec. Increase of the ac field strength leaves the high-frequency dispersion relatively unaffected while causing a complete change in the lower region: the loss maximum flattens and moves to lower frequencies, the plateau of the low-frequency permeability is raised from 130 to *ca* 1300, and a pronounced nonlinearity of the magnetization process is observed.

These facts tend to indicate that the lower peak is caused by a reversible wall oscillation, and that at higher field strength the walls tear loose from their anchored position and traverse the material in widening swings.

[43] Supplied through courtesy of Linde Air Products Company.
[44] Galt, Andrus, and Hopper, Revs. Modern Phys. **25**, 93 (1953).

Temperature Effects

Lowering the temperature of the ceramics produces a very striking effect (Figs. 7.5 and 7.6): a broad relaxation spectrum splits off from the main dispersion region and moves rapidly to lower frequencies; simultaneously, two loss peaks become clearly discerned in the range from 10^8 to 10^{10} cps. A corresponding change occurs in the magnetic spectrum of the single crystal (Fig. 7.7).

A detailed study of the relaxation spectrum[45] shows that it stems from some process requiring an activation energy U. The frequency ω_m at which the maximum of the loss tangent is traversed, varies with temperature as

$$\omega_m = \omega_0 e^{-U/kT}, \tag{7.8}$$

and a Cole-Cole plot places all measurements on circular arcs with centers below the real axis (Fig. 7.8).‡

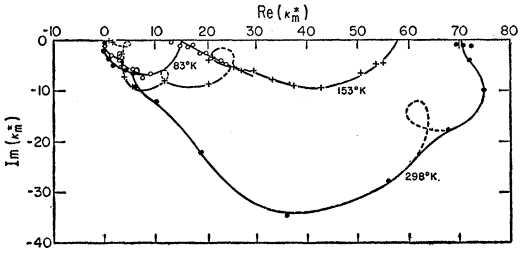

FIG. 7.6. Cole-Cole plot for data of Fig. 7.5 ($Ni_{0.9}Zn_{0.1}Fe_2O_4$).

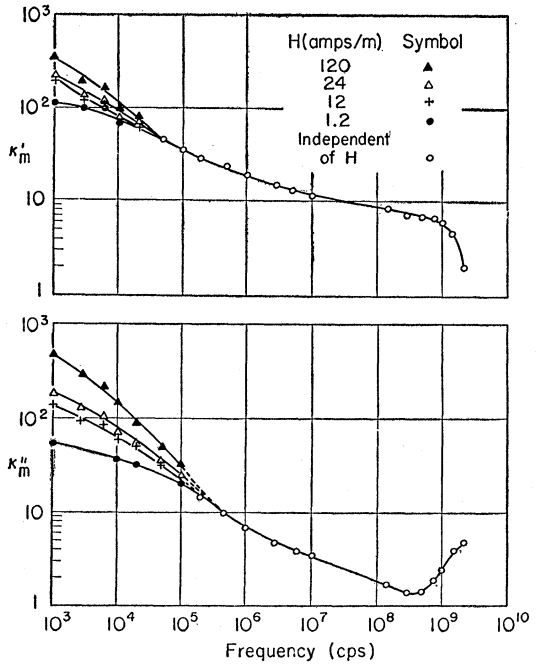

FIG. 7.7. Magnetic spectrum of a nickel ferrite single crystal at 83°K.

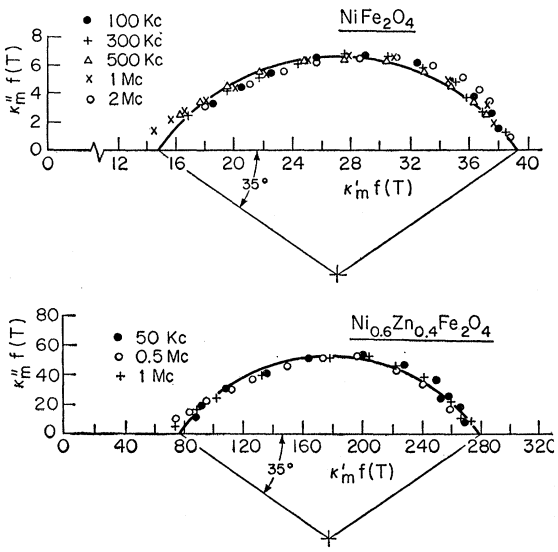

FIG. 7.8. Cole-Cole plot of relaxation spectra for nickel-zinc ferrite ceramics (Epstein[45]).

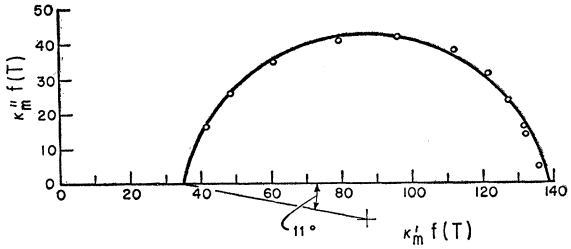

FIG. 7.9. Cole-Cole plot of relaxation spectrum for nickel ferrite crystal (Epstein[45]).

The data for ceramics are fitted by a distribution of time constants extending over two decades. This is not surprising because individual crystallites differ in composition and state of oxidation, in strain and environment. This is confirmed by measurements on the nickel ferrite single crystal which give a distribution of time constants about thirty times narrower than that for the corresponding ceramic (Fig. 7.9).

Activation energies obtained from these data (Table 7.1) agree well with those of conductivity measurements, and with previous findings of Wijn.[23,46] Temperature has a very striking influence on the switching of memory cores made from these materials: while at room temperature the switching takes place in less than 10^{-6} sec, Epstein[45] observed time constants of seconds at 77°K. This corresponds to the damping effects seen by Galt[47] in domain-wall motion studies on single crystals, where at these low temperatures the apparent

[45] D. J. Epstein, Sc.D. thesis, Massachusetts Institute of Technology, May, 1956.

‡ The relaxation spectrum can be traversed either by varying the frequency at fixed temperature, or by temperature variation at fixed frequency. In the latter case the range of the relaxation dispersion ($\kappa_{ms}' - \kappa_{m\infty}'$) is found to vary with temperature. The function $f(T)$ appearing in Fig. 7.8 is an empirical factor introduced to compensate for this change.

[46] H. P. J. Wijn and H. van der Heide, Revs. Modern Phys. **25**, 98 (1953).

[47] J. K. Galt, Bell System Tech. J. **33**, 1023 (1954); *ibid.* **34**, 439 (1955).

TABLE 7.1. Activation energies for conduction and magnetic relaxation in nickel-zinc ferrite (Epstein[45]).

Composition	Activation energies (ev) Conductivity 170°K	Magnetic relaxation
$NiFe_2O_4$	0.14	0.17
$Ni_{0.8}Zn_{0.2}Fe_2O_4$	0.14	0.12
$Ni_{0.6}Zn_{0.4}Fe_2O_4$	0.16	0.17
$Ni_{0.3}Zn_{0.7}Fe_2O_4$	0.14	0.13

damping constants were increased by orders of magnitude.

Direct comparison of our results with those of the Philips Research Laboratories is misleading, if we assume that both parties, when quoting a ferrite composition of the same stoichiometry, speak about the same material. As already pointed out in Sec. 5, our ceramic samples were fired to within a few percent of theoretical density, while the Philips Feroxcube materials are fired at lower temperature and maintain a porous structure. The consequences for domain-wall motion are decisive: in the porous material the walls are easily trapped and immobilized and porous ceramics re-oxidize more completely on cooling, hence are much less conducting. Thus the Philips ceramics may show the relaxation spectrum identified here only to a minor degree, or not at all.

Origin of the Relaxation Spectrum

All of our measurements thus far are consistent with the following interpretation of the relaxation spectrum.

In slightly reduced ferrites Fe^{2+} and Fe^{3+} cations are built in at octahedral lattice sites and can easily exchange electrons, as is known from studies on magnetite. Transfer of electrons also represents a transfer of magnetic spins. The domain-wall array in a crystal corresponds to some minimum free-energy constellation. Without conductivity a wall is therefore trapped in a potential minimum; with conductivity, a deeper, more favorable, minimum can be created by shifting of magnetic moments. This is a kind of aging effect observed in metals, for example, as a diffusion of carbon or nitrogen to alternate interstitial sites.[48] In our case, since electrons are being shifted, the diffusion is much more rapid; at room temperature the wall buries itself in about 10^{-9} sec. As the temperature is lowered, the electron exchange is slowed and the domain wall needs more and more time to deepen its potential well.

Application of an oscillatory field causes a wall to move up the sides of its well; the electron atmosphere tends to follow this swing by a redistribution of the Fe^{2+}-Fe^{3+} arrangement. If the period of oscillation is long in comparison to the electron diffusion time, the wall behaves as if oscillating in a shallow well not deepened by electron interchange. This seems to be the situation at room temperature, where the wall resonance appears unimpeded by electron drag. Lowering the temperature and thus lengthening the relaxation time of the electron atmosphere, causes the wall resonance to degenerate into a relaxation spectrum controlled by electron-spin redistribution. At very low temperatures, when the electrons are essentially immobilized in the room-temperature-resonance region, a wall resonance should reappear at a higher frequency, since the wall oscillation now corresponds to a motion in the deepened well.

Two other considerations support the interpretation that the low-frequency loss peak is due to domain-wall motion rather than to domain rotation. Effective internal fields of the order of 240 to 2400 amp/m (3 to 30 oersteds) are required to account for gyromagnetic resonances in the range of 10^7 to 10^8 cps. Although such low fields might result from a near balance of shape and anisotropy effects, such a balance is improbable. Furthermore, the Landau-Lifshitz dispersion formula predicts that for increased damping, a gyromagnetic resonance should tend towards a relaxation spectrum at frequencies much greater than those of the original position; this is in contrast to our observations.

Origin of the Magnetic Dispersion between 10^8 and 10^{11} cps

The dispersion and loss peak resolved between 10^9 and 10^{10} cps in the room-temperature spectra of nickel-

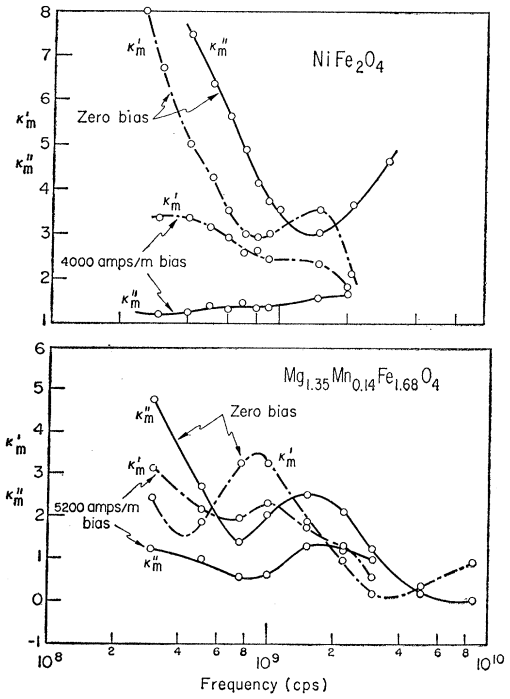

Fig. 7.10. Effect of static magnetic field on frequency response of nickel ferrites.

[48] J. L. Snoek, Physica **8**, 711 (1941); L. Néel, J. phys. radium **13**, 249 (1952); A. M. Clogston, Bell System Tech. J. **34**, 739 (1955).

zinc ferrites is clearly a resonance, and in nickel ferrite the high frequency limit is in good agreement with that predicted for a gyromagnetic resonance in the presence of domain walls (Sec. 6b). This appears therefore to be the correct interpretation. The origin of the loss peak between 10^8 and 10^9 cps which develops out of the low-frequency dispersion as the temperature is lowered (Fig. 7.5) is less clear. It could be the re-emerging wall resonance referred to in the previous section, but more probably it is a group of gyromagnetic resonance produced when excitation takes place perpendicular to domain walls. In the simple case treated in Sec. 6b, excitation perpendicular or parallel to such walls gives two resonances separated by a frequency interval of the order of $\gamma\mu_0 M/2$ (5×10^9 cps for nickel ferrite). The observed separations of the two peaks are somewhat smaller, but this might be accounted for by a more realistic domain configuration.

Effect of Biasing Field

Application of a static magnetic field parallel to the oscillatory field markedly affects the lower resonance region (Fig. 7.10). The prominent minimum in κ_m' near 10^9 cps practically disappears, indicating that it was caused by the high-frequency tail of the lower dispersion. This behavior is consistent with the idea that this part of the dispersion is due to, or greatly influenced by, the presence of domain walls. In particular, the selective elimination of walls oriented perpendicularly to the oscillatory field would explain the reduction of the lower group of spin resonances whose position is determined by their presence.

Cation Substitution

The effect of cation substitution on magnetic spectra is not a simple one, since the fundamental properties

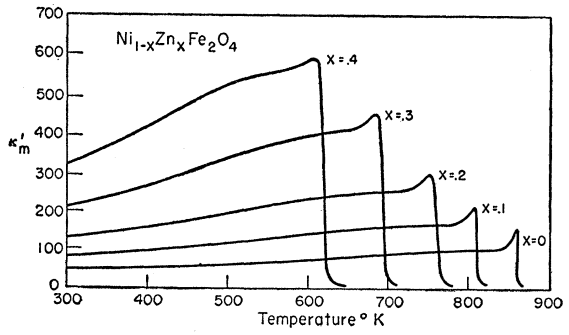

FIG. 7.11. Temperature dependence of initial permeability for nickel-zinc ferrites (10^8 cps).

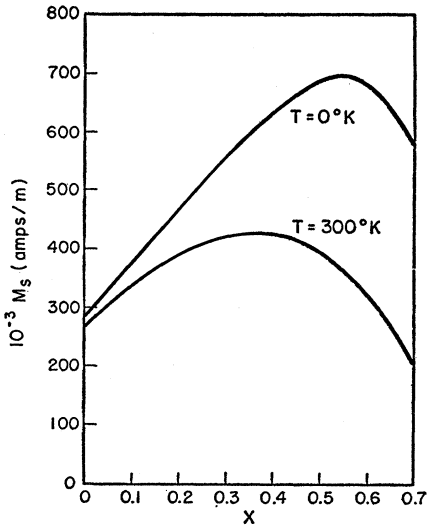

FIG. 7.12. Saturation magnetization for the nickel-zinc ferrite series.

of the material, such as saturation magnetization, Curie point, anisotropy, magnetostriction, conductivity, domain and grain structure, undergo changes. The temperature dependence of the initial permeability for the nickel-zinc ferrite series (Fig. 7.11) reflects relatively clearly that the Curie temperature decreases with increasing zinc content and that anisotropy and magnetostriction decrease as the Curie point is approached. The saturation magnetization, on the other hand, traverses a maximum and then falls to zero for zinc ferrite (Fig. 7.12).[49] The dispersion between 10^8 and 10^{10} cps, in a general way, adjusts to this change in magnetization by a shift in resonance frequency, but does not behave as simple theory would predict. This is probably due to variations in the other parameters and their effect on domain patterns and interactions.

It is obvious that we are still far from a complete understanding of these ferromagnetics. Many pieces of the puzzle, however, have been identified, and dielectric spectroscopy is one approach of assembling them in proper perspective.

ACKNOWLEDGMENTS

We wish to thank our co-workers, Professor D. J. Epstein and Dr. R. D. Waldron, whose contributions have been indicated in the text, for helpful discussions, and Mr. J. Kalnajs for his investigation of the optical properties of magnetite films.

[49] E. W. Gorter, Nature **165**, 798 (1950); C. Guillaud, J. phys. radium **12**, 143 (1951); R. Pauthenet, Ann. phys. [12] **7**, 714 (1952).

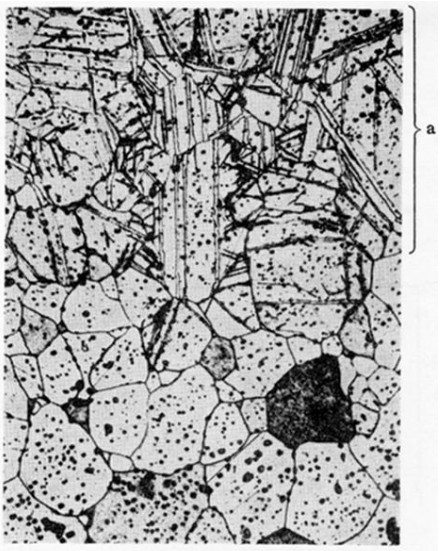

FIG. 5.11. Highly resistive surface layer (a) of manganese-zinc ferrite.